



**Universität
Zürich^{UZH}**



The XENONnT direct dark matter detection experiment: assembly and commissioning.

Giovanni Volta, PhD student

Zurich PhD student seminar

September 9th, 2020

Outline

1. THE XENON_nT EXPERIMENT
2. TIME PROJECTION CHAMBER ASSEMBLY
3. DETECTOR COMMISSIONING
4. SUMMARY AND OUTLOOK

The XENON project

Located at Laboratori Nazionali del Gran Sasso (Italy), the XENON project aims at the direct detection of dark matter particles deploying a low-radioactivity detector consisting on dual-phase time projection chamber filled with liquid xenon.



12 countries



28 institution



~ 160 scientists

15 kg
0.87 kg × yr

2005

XENON10

2007



161 kg
48 kg × yr

2009

XENON100

2016



3.2 tonnes
1 t × yr

2019

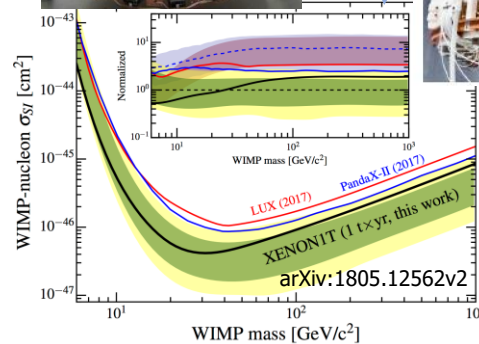
XENON1T



8.4 tonnes
20 t × yr

2023

XENONnT

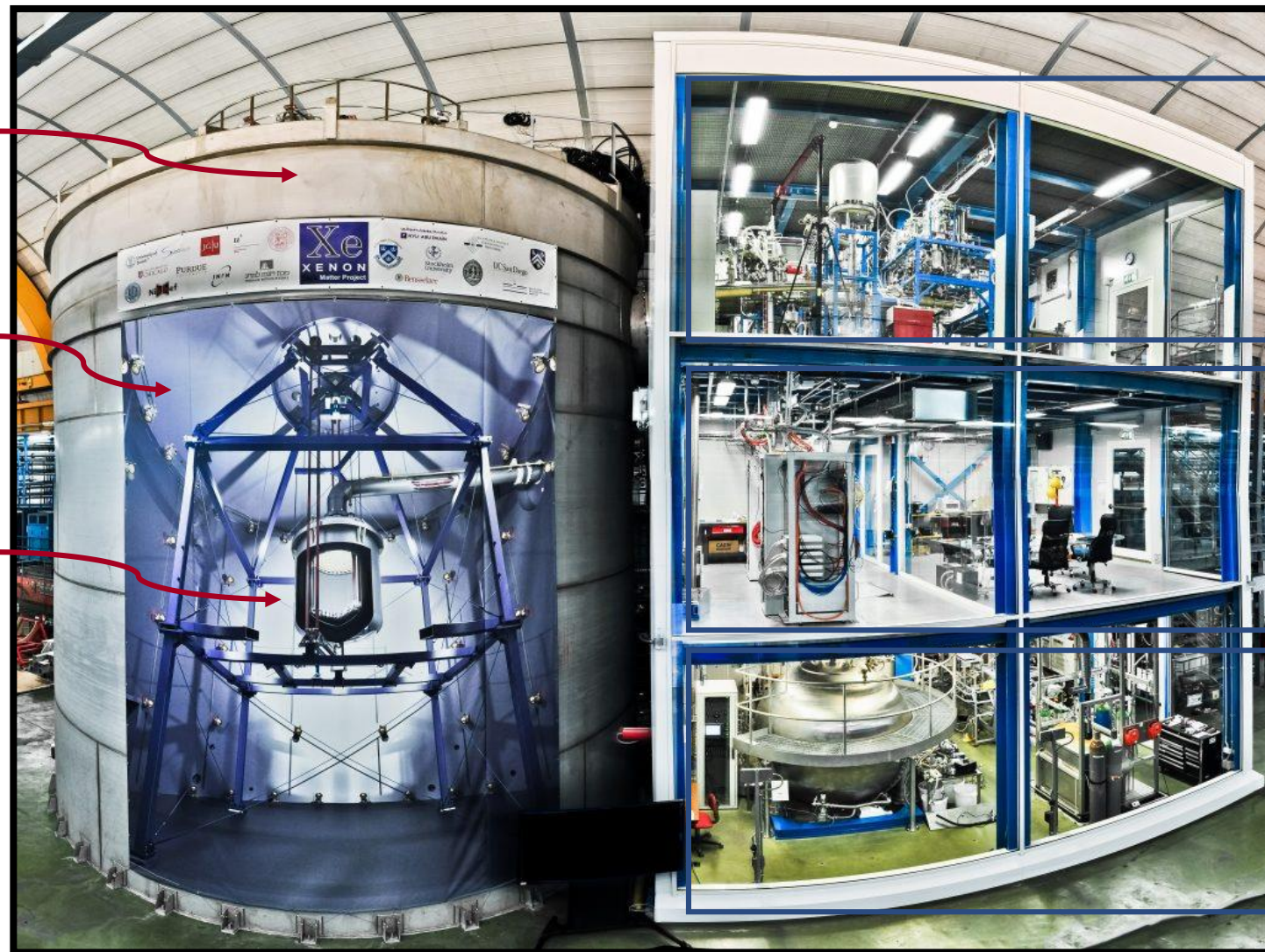


The XENONnT experiment

Cylindrical (10.2×9.6) m stainless-steel water tank

Inner neutron veto, optically separated by the outer Cherenkov muon veto

The central liquid xenon (LXe) dual-phase time projection chamber (TPC)



Cryogenics and Purification systems

DAQ and Slow Control

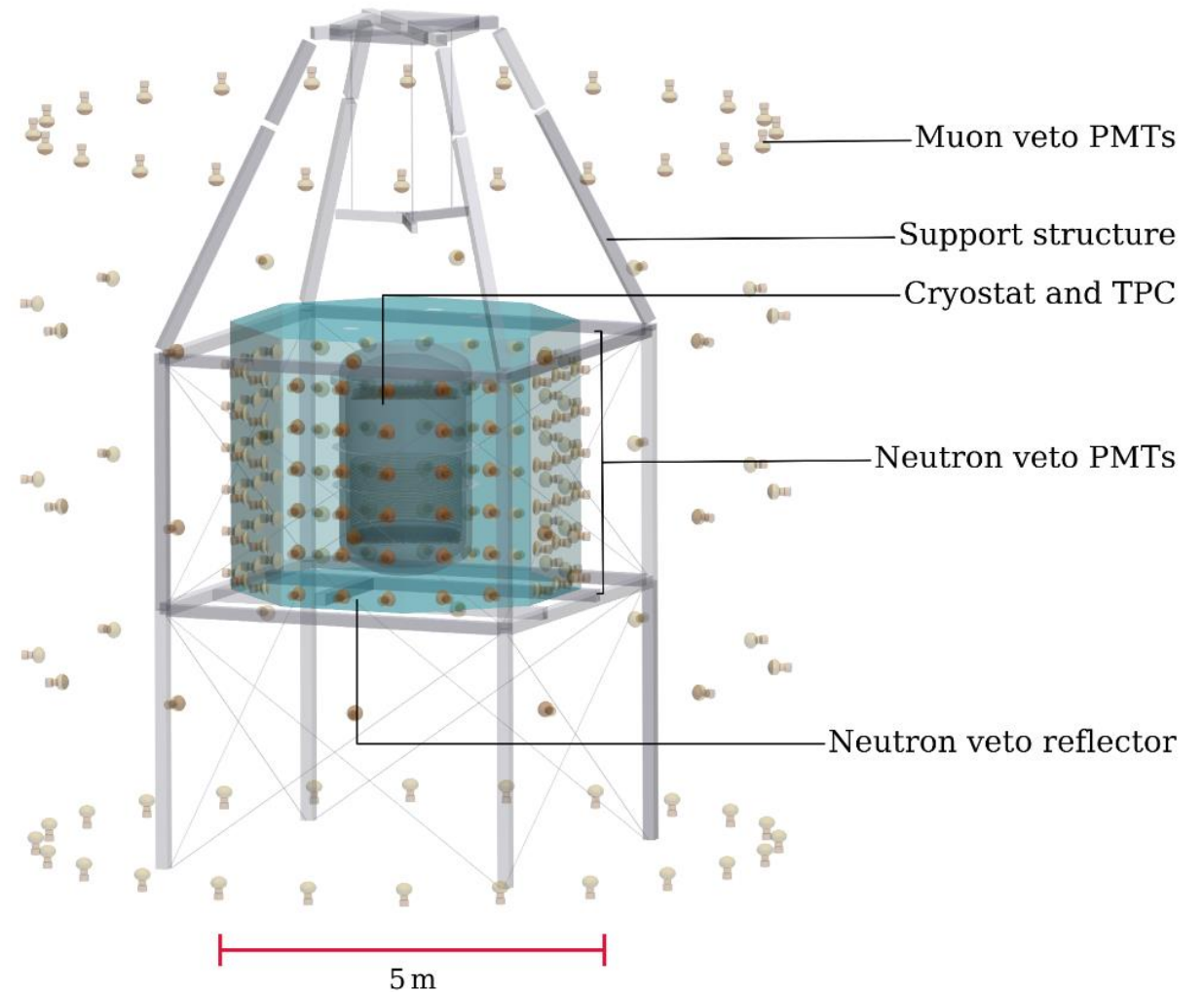
Xenon Storage and Recovery

The neutron veto

- To reduce radiogenic neutron background by tagging event in coincidence between the TPC and the neutron veto.
- 120 Hamamatsu R5912-100-10 8" placed along reflective panels around the cryostat.
- Water with $\sim 0,2\%$ gadolinium concentration to enhance neutron capture.

The muon veto

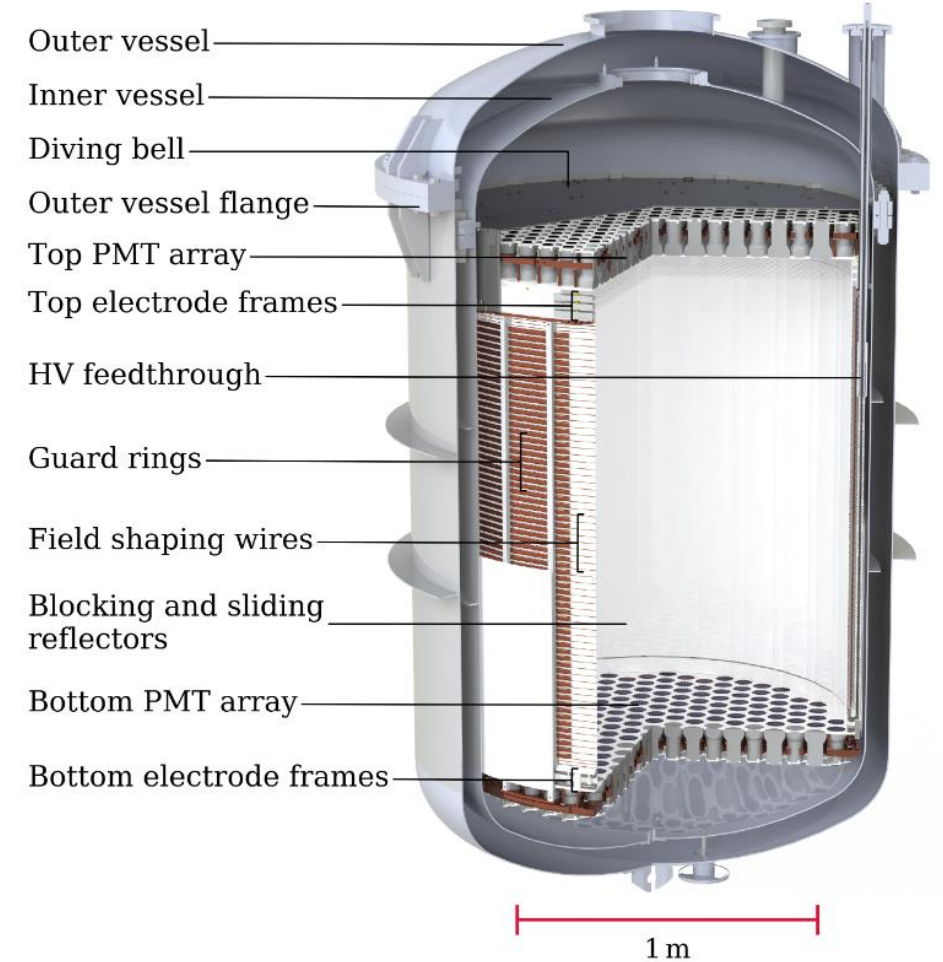
- ≈ 700 tonnes of Gd-loaded pure water
- 84 Hamamatsu R5912ASSY 8" PMTs
- Active Cherenkov veto for tagging incoming muon and hadronic showers
- Effective shielding against environmental radiation



arXiv:2007.08796v1

The dual-phase LXe TPC

- 5.9 t of LXe as active region, enclosed by 24 polytetrafluoroethylene (PTFE) reflector panels.
- PMT array at the top (253) and at the bottom (241) of the active region.
- 3" Hamamatsu R11410-21 PMT: low radioactivity and high quantum efficiency.
- Electric field generated between a top gate electrode and a bottom cathode (148,5 cm a part). An anode electrode is placed in the GXe, 8 mm above the gate.
- PMT arrays protected from the field by two adjacent screening electrodes.
- Electric field uniformity achieved by two concentric sets of OFHC copper field shaping rings: guard rings and field shaping wires.

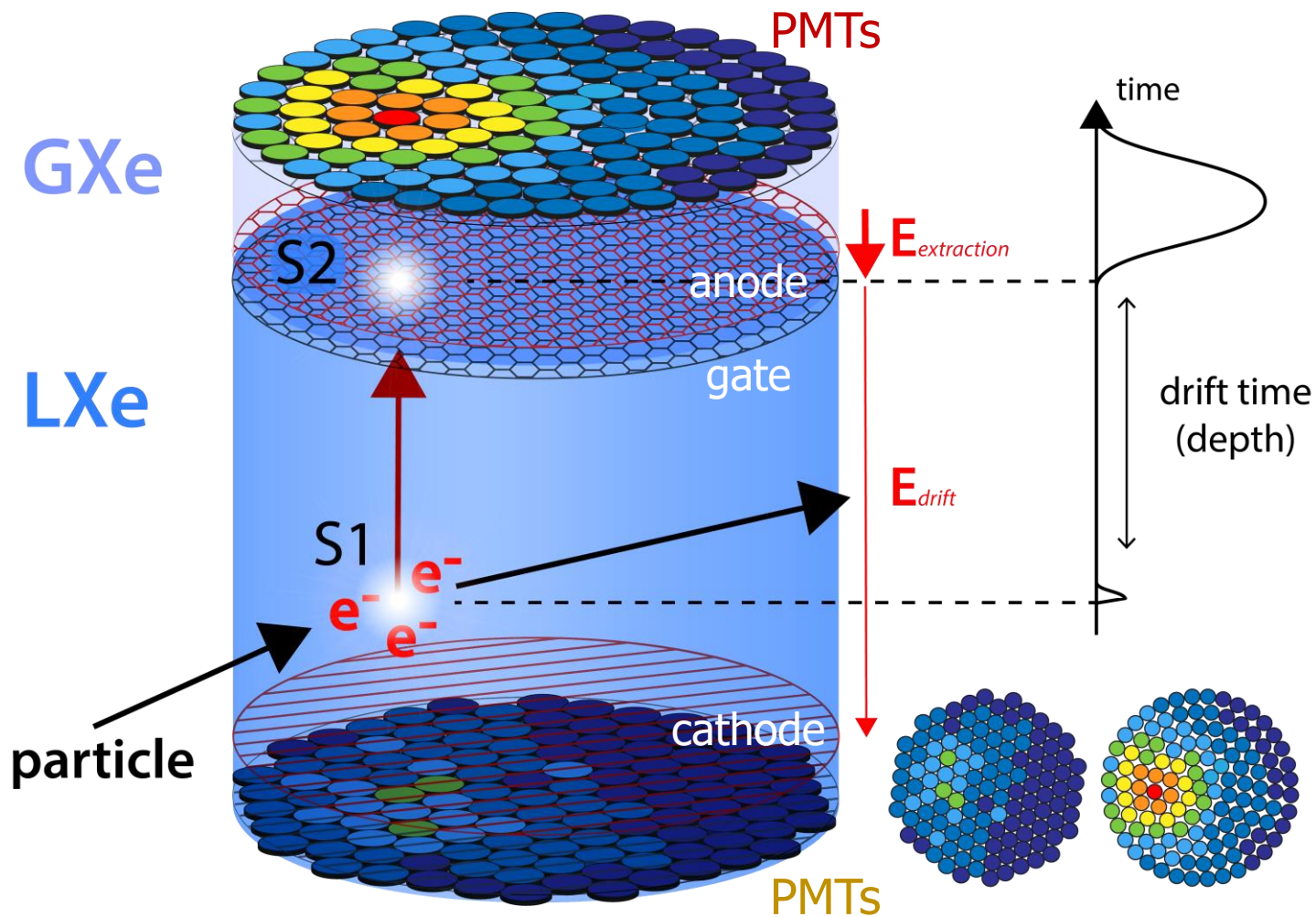


arXiv:2007.08796v1

Two-phase TPC operating principle:

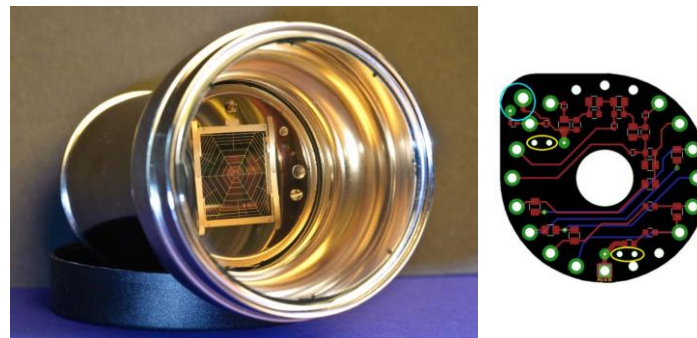
- Particle interaction causes primary scintillation light **S1** and ionisation of xenon atoms.
- Secondary light emission **S2** in the gas phase from the drifted charged.

1. Energy reconstructed from (**S1**; **S2**)
2. (x; y) event position obtained from top PMTs hit pattern
3. Z position computed from **S2-S1** time difference
4. Particle discrimination from **S2/S1** ratio



The XENONnT photosensors

- Hamamatsu PMT, type R11410-21.
- Voltage divider circuit to operate PMT developed at UZH: scheme adopted with grounded anode and negative biased photocathode ($R_{\text{total}} = 92.5 \text{ M}\Omega$).
- Accuglass 30 AWG TYP28-30 Kapton insulated ultra-high vacuum cables for the HV and Ground connection, PTFE-insulated coaxial RG196 for signal cables.
- Screening campaign with low-background germanium spectrometer (e.g. Gator) for every components.
- 109 PMTs tested using MarmotX facility at UZH. Performance characterization in gas and liquid xenon:
 - Gain and DC rate
 - After pulse spectrum
 - Light emission



R11410-21 PMT and voltage divider circuit.

PMTs gain distribution

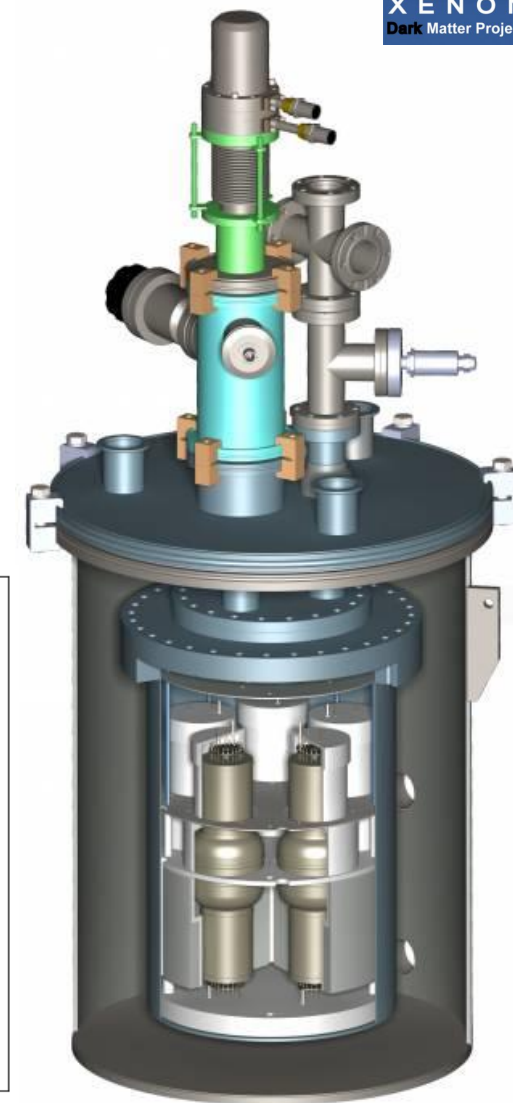
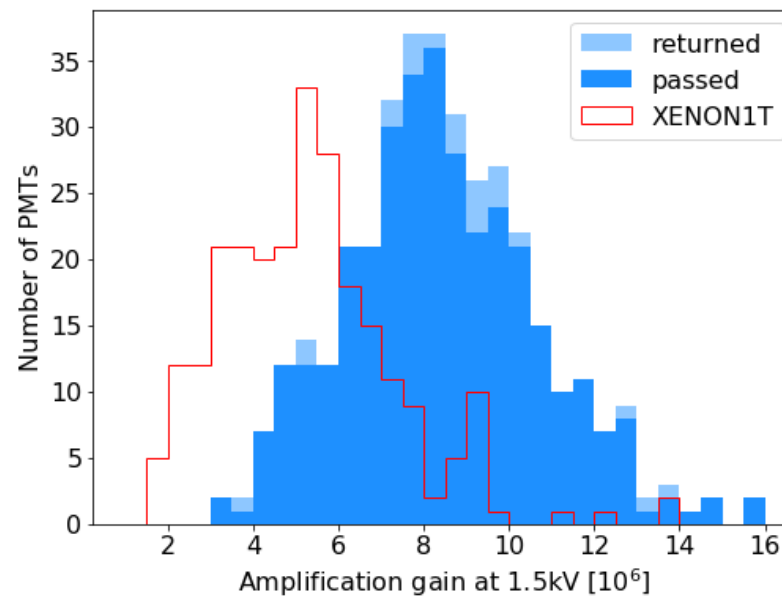


Illustration of the MarmotX testing facility.

PMT array assembly

The two PMT arrays have been assembled in advance with 253 PMTs on the top and 241 in the bottom array.

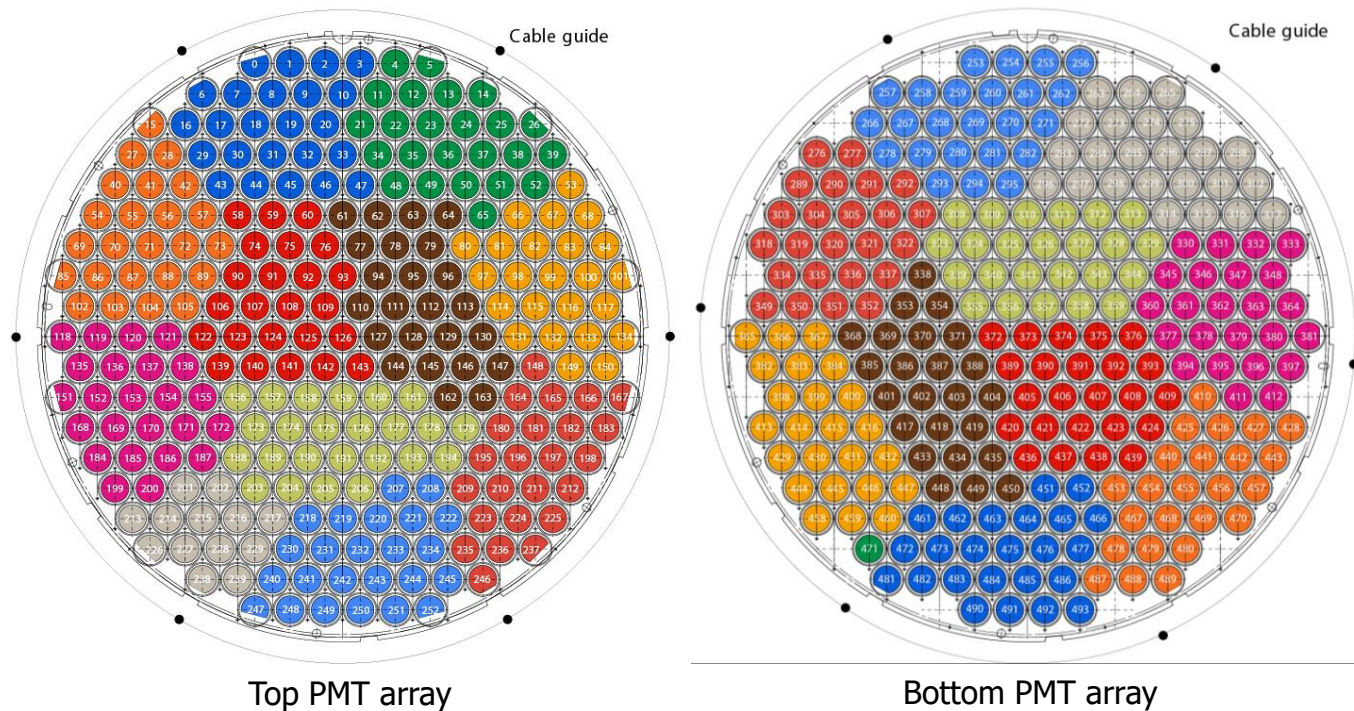
- Every component has been cleaned with different procedures depending by the material.
- The PMTs have been placed following a cabling plan where the arrays have been divided into 21 sectors (11 in the top array and 10 in the bottom array) with a maximum of 24 PMTs each.
- The arrays have been stored in a clean environment under flowing nitrogen atmosphere to prevent external contamination.



PMT array assembly

The two PMT arrays have been assembled in advance with 253 PMTs on the top and 241 in the bottom array.

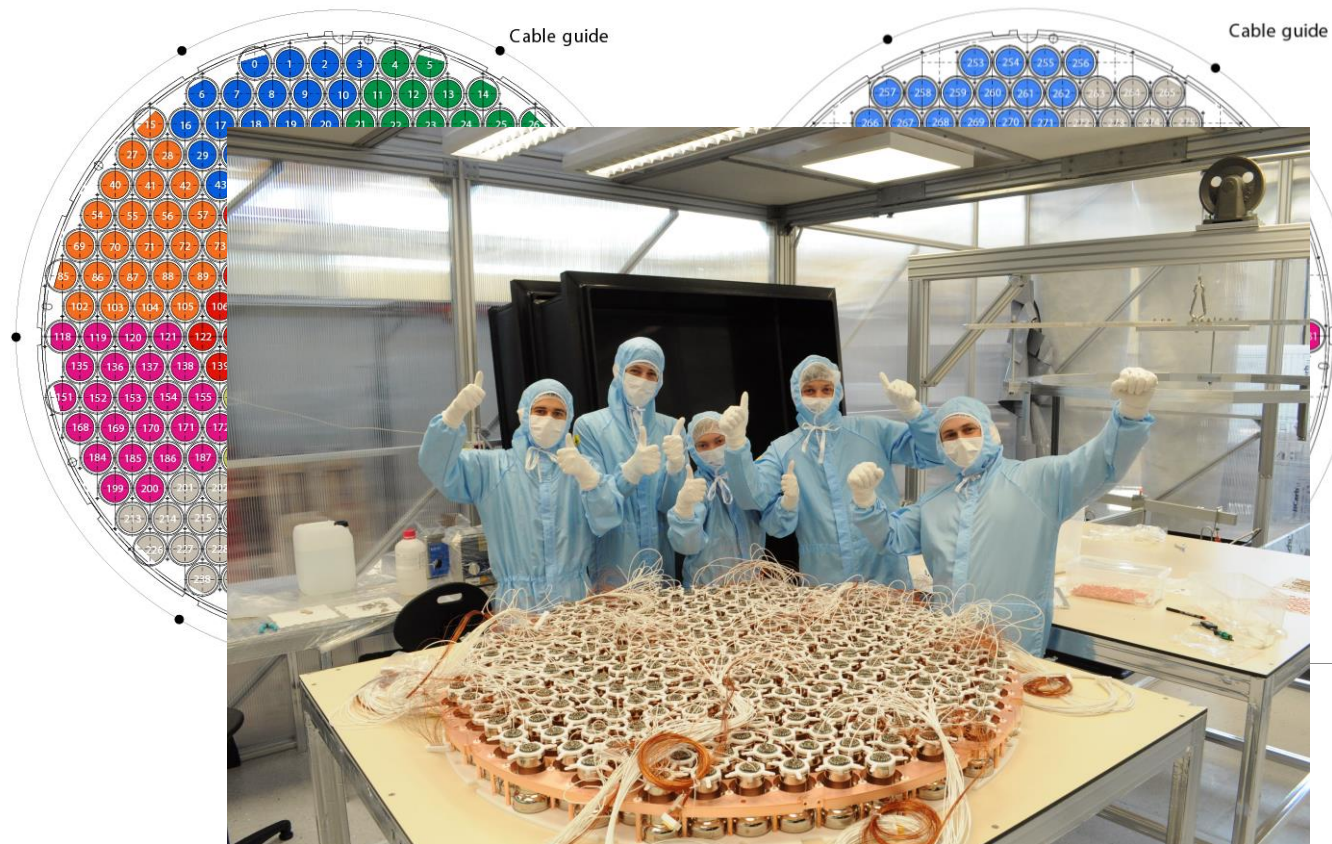
- Every component has been cleaned with different procedures depending by the material.
- The PMTs have been placed following a cabling plan where the arrays have been divided into 21 sectors (11 in the top array and 10 in the bottom array) with a maximum of 24 PMTs each.
- The arrays have been stored in a clean environment under flowing nitrogen atmosphere to prevent external contamination.



PMT array assembly

The two PMT arrays have been assembled in advance with 253 PMTs on the top and 241 in the bottom array.

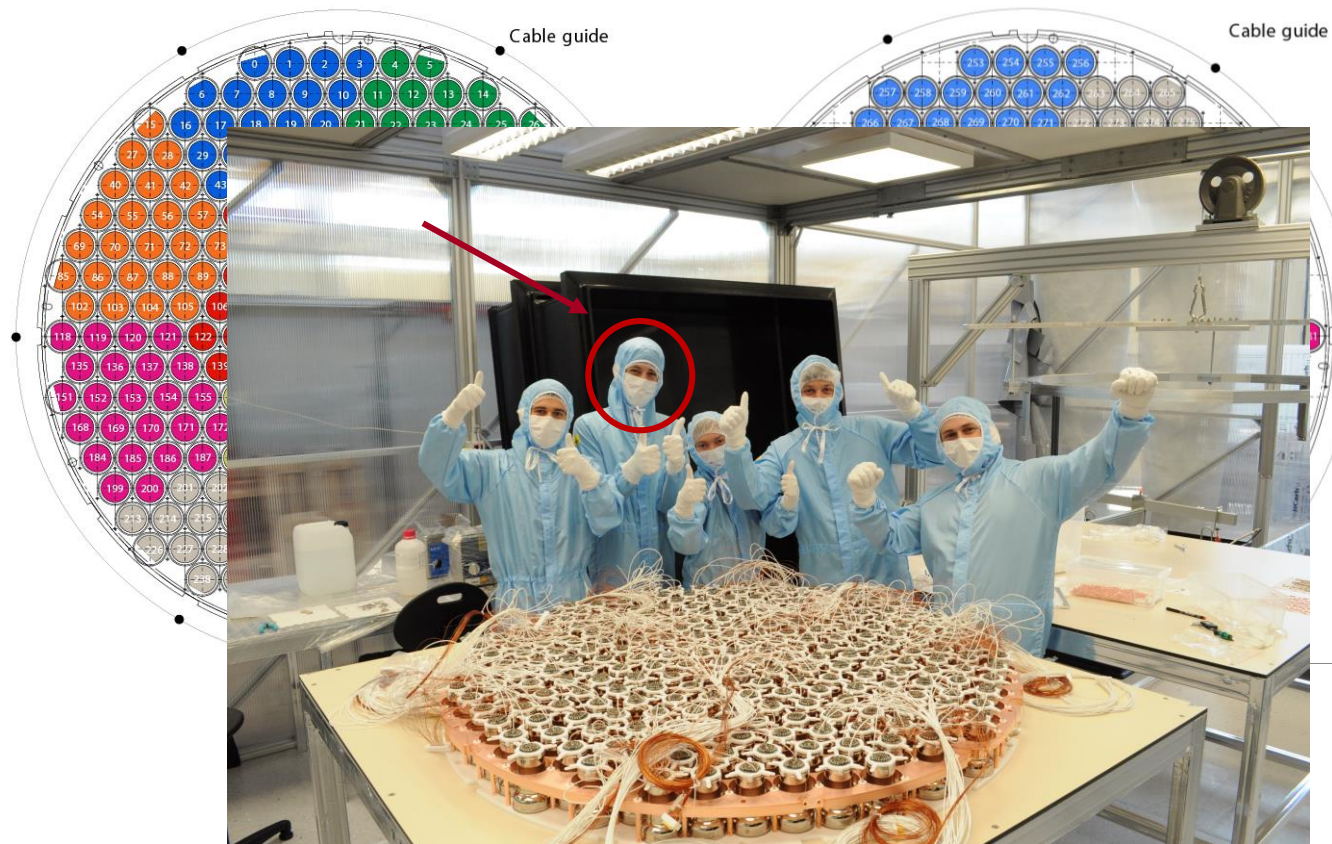
- Every component has been cleaned with different procedures depending by the material.
- The PMTs have been placed following a cabling plan where the arrays have been divided into 21 sectors (11 in the top array and 10 in the bottom array) with a maximum of 24 PMTs each.
- The arrays have been stored in a clean environment under flowing nitrogen atmosphere to prevent external contamination.



PMT array assembly

The two PMT arrays have been assembled in advance with 253 PMTs on the top and 241 in the bottom array.

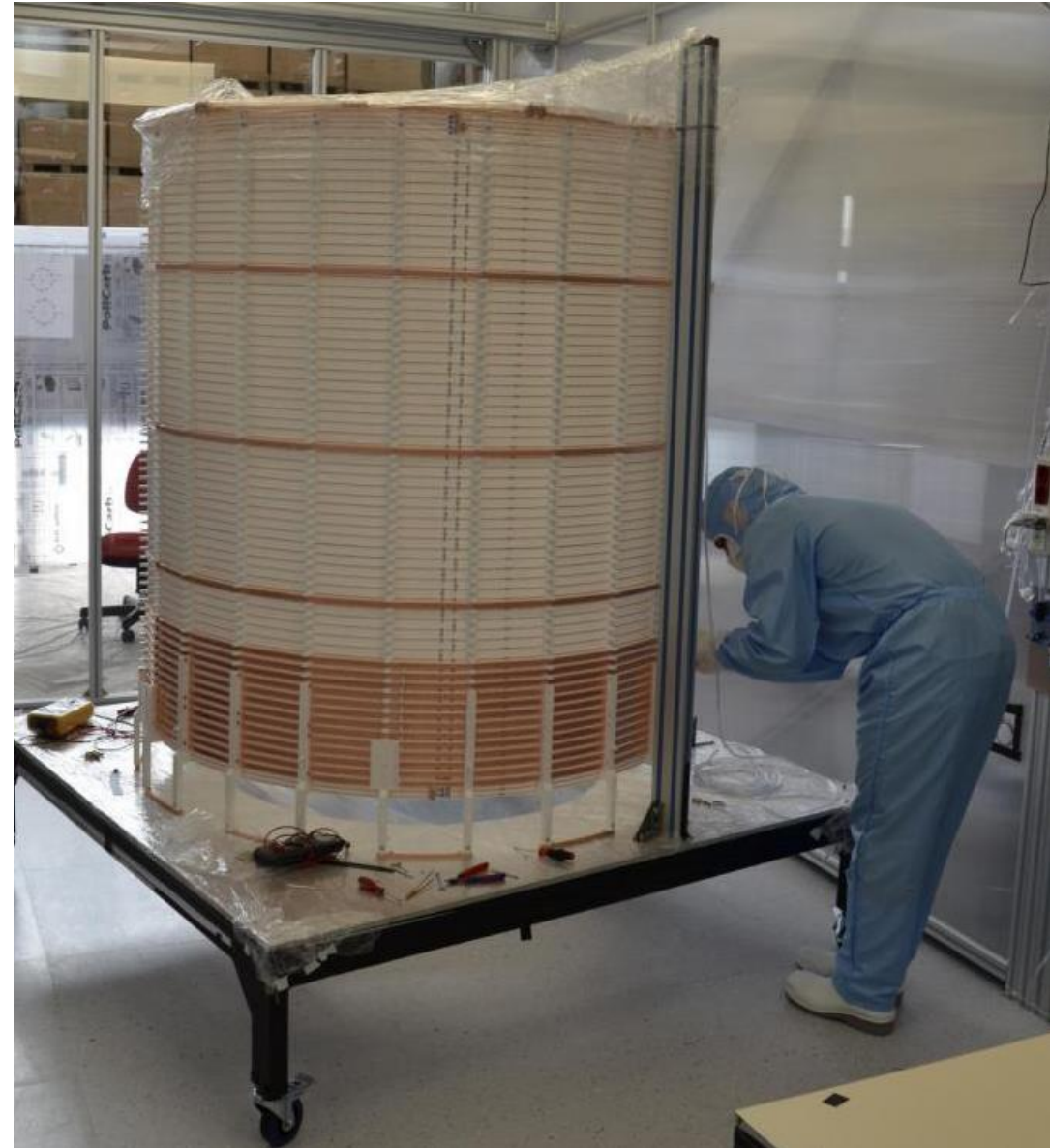
- Every component has been cleaned with different procedures depending by the material.
- The PMTs have been placed following a cabling plan where the arrays have been divided into 21 sectors (11 in the top array and 10 in the bottom array) with a maximum of 24 PMTs each.
- The arrays have been stored in a clean environment under flowing nitrogen atmosphere to prevent external contamination.



TPC assembly above ground

The assembly of the TPC was carried out at LNGS from February 24th to March 5th, during 10 intense days.

- PTFE support structure with 48 panels which define the inner region of the detector.
- 71 field shaping rings and 64 copper rings, connected using two independent resistor chains, for electric field uniformity.
- 10 (400-2400) nm transmitting silica fibers for the light calibration system.
- Two screening electrodes, cathode, gate and anode.



TPC assembly above ground

The assembly of the TPC was carried out at LNGS from February 24th to March 5th, during 10 intense days.

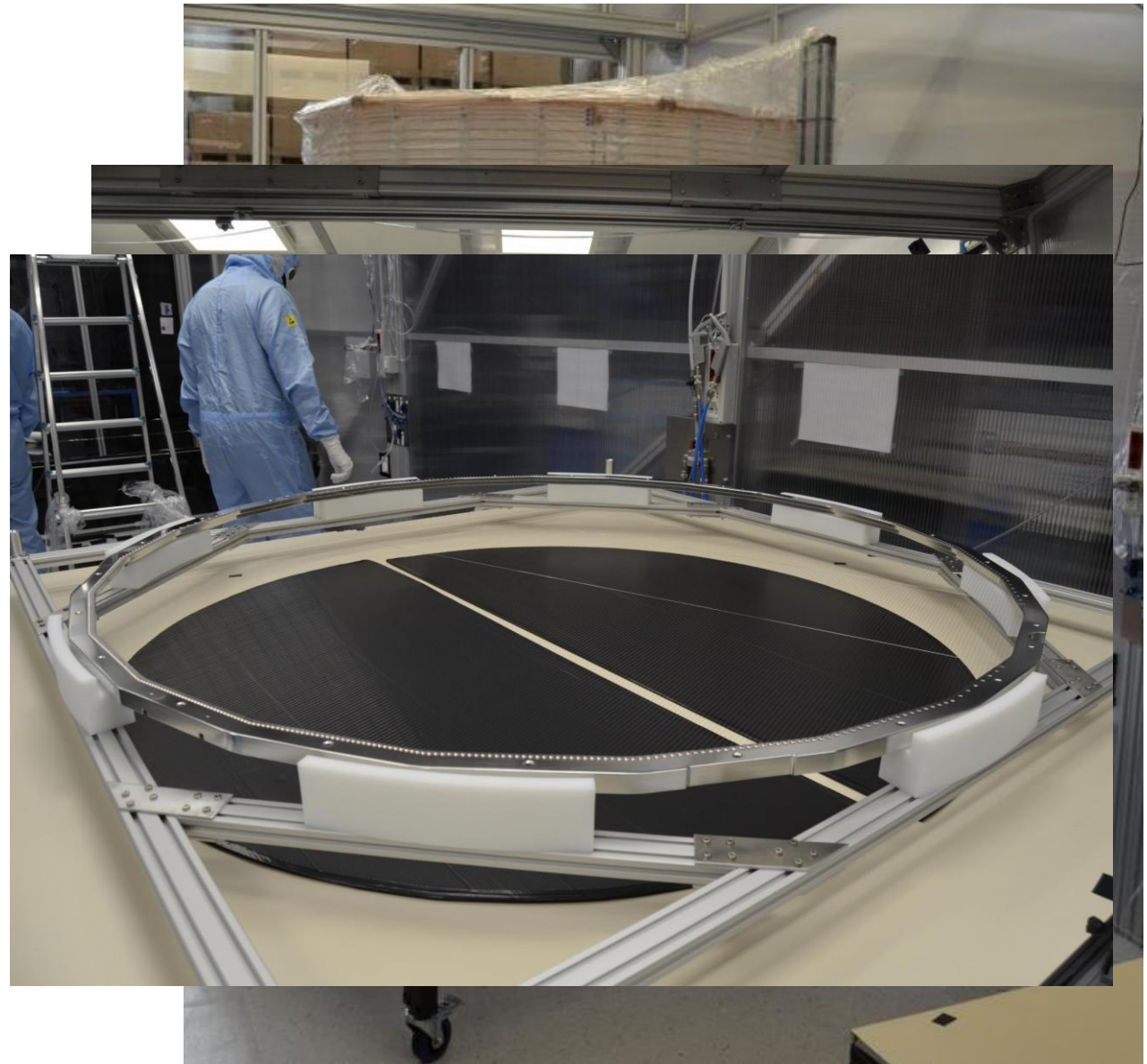
- PTFE support structure with 48 panels which define the inner region of the detector.
- 71 field shaping rings and 64 copper rings, connected using two independent resistor chains, for electric field uniformity.
- 10 (400-2400) nm transmitting silica fibers for the light calibration system.
- Two screening electrodes, cathode, gate and anode.



TPC assembly above ground

The assembly of the TPC was carried out at LNGS from February 24th to March 5th, during 10 intense days.

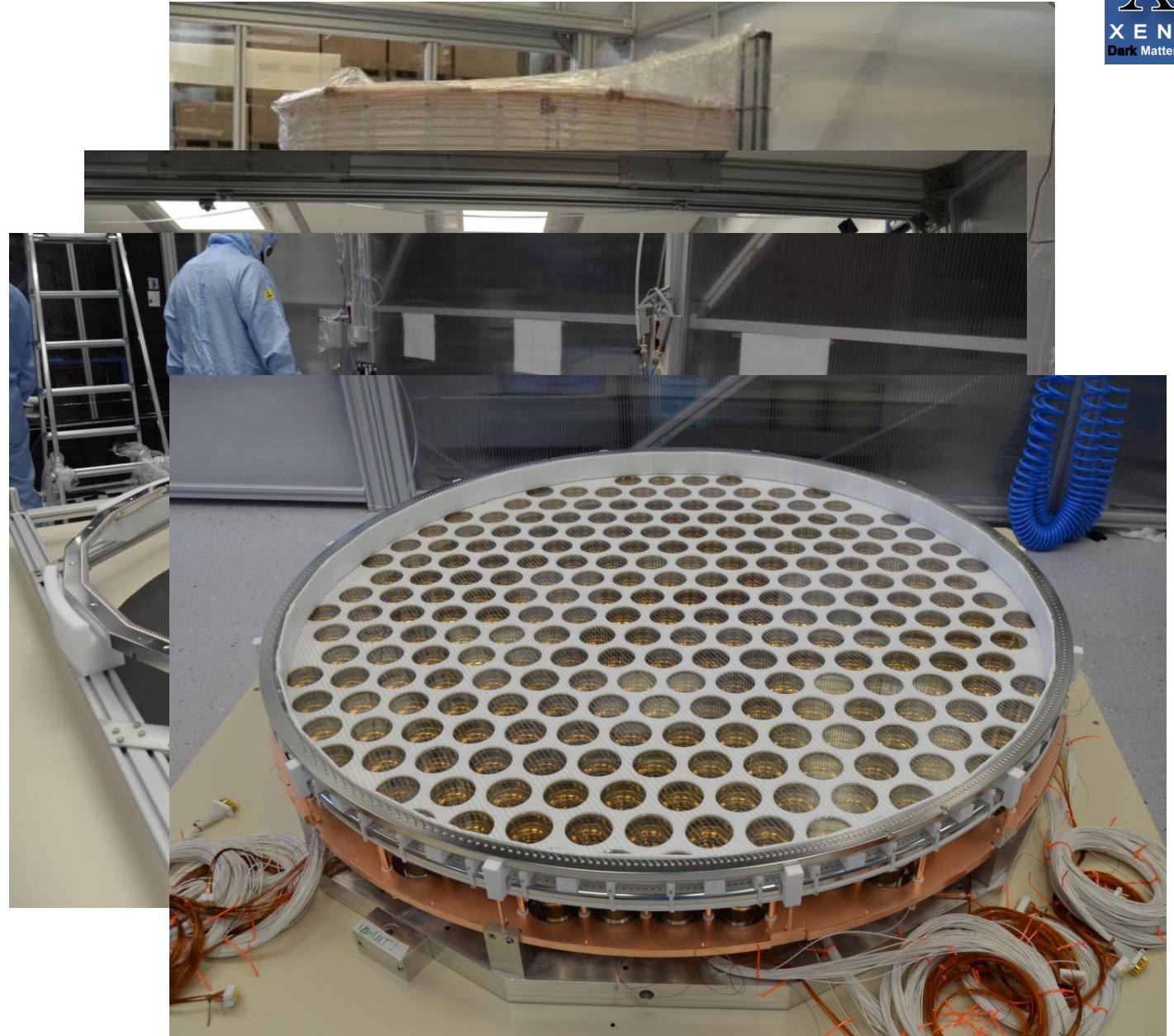
- PTFE support structure with 48 panels which define the inner region of the detector.
- 71 field shaping rings and 64 copper rings, connected using two independent resistor chains, for electric field uniformity.
- 10 (400-2400) nm transmitting silica fibers for the light calibration system.
- Two screening electrodes, cathode, gate and anode.



TPC assembly above ground

The assembly of the TPC was carried out at LNGS from February 24th to March 5th, during 10 intense days.

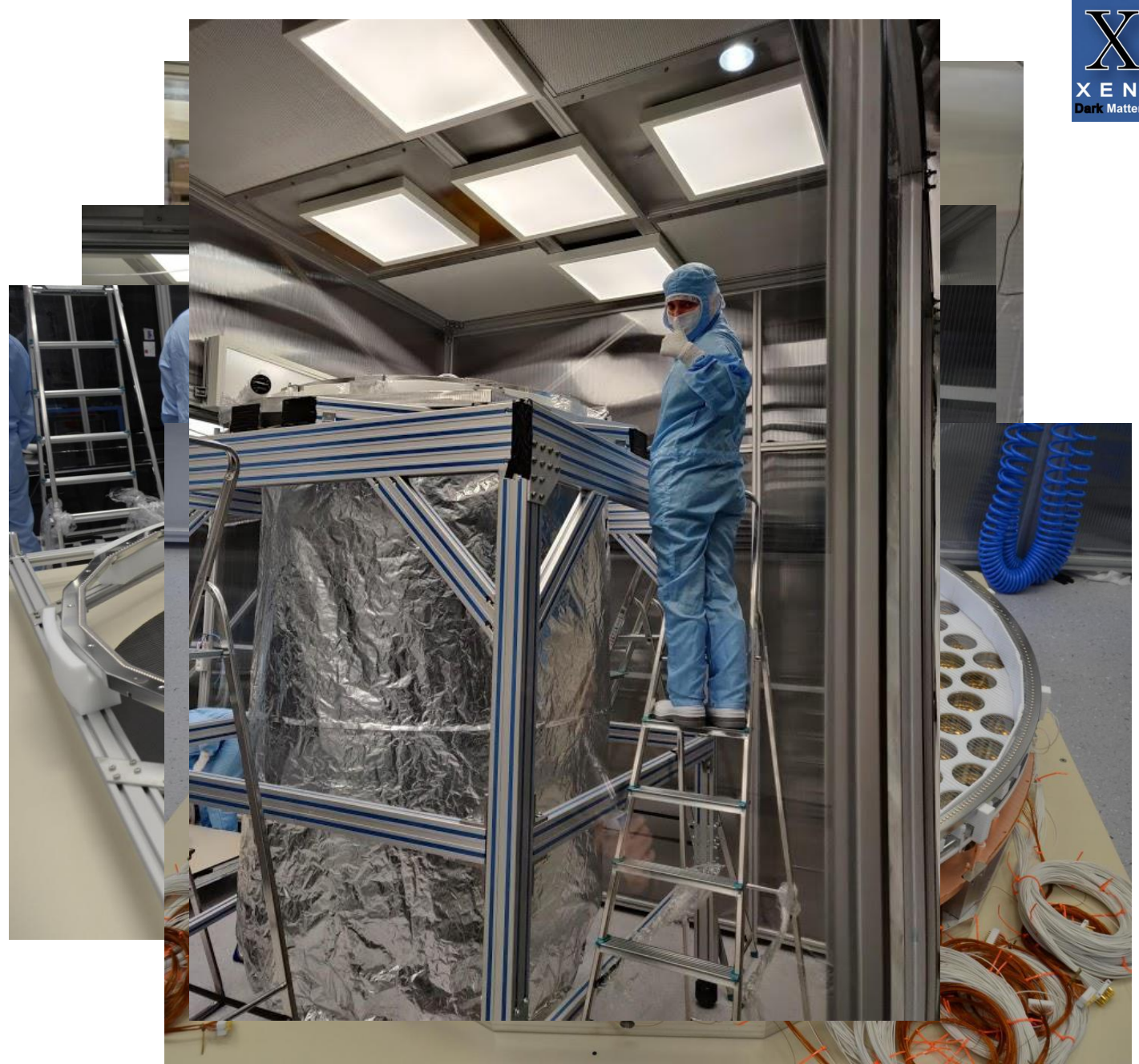
- PTFE support structure with 48 panels which define the inner region of the detector.
- 71 field shaping rings and 64 copper rings, connected using two independent resistor chains, for electric field uniformity.
- 10 (400-2400) nm transmitting silica fibers for the light calibration system.
- Two screening electrodes, cathode, gate and anode.



TPC assembly above ground

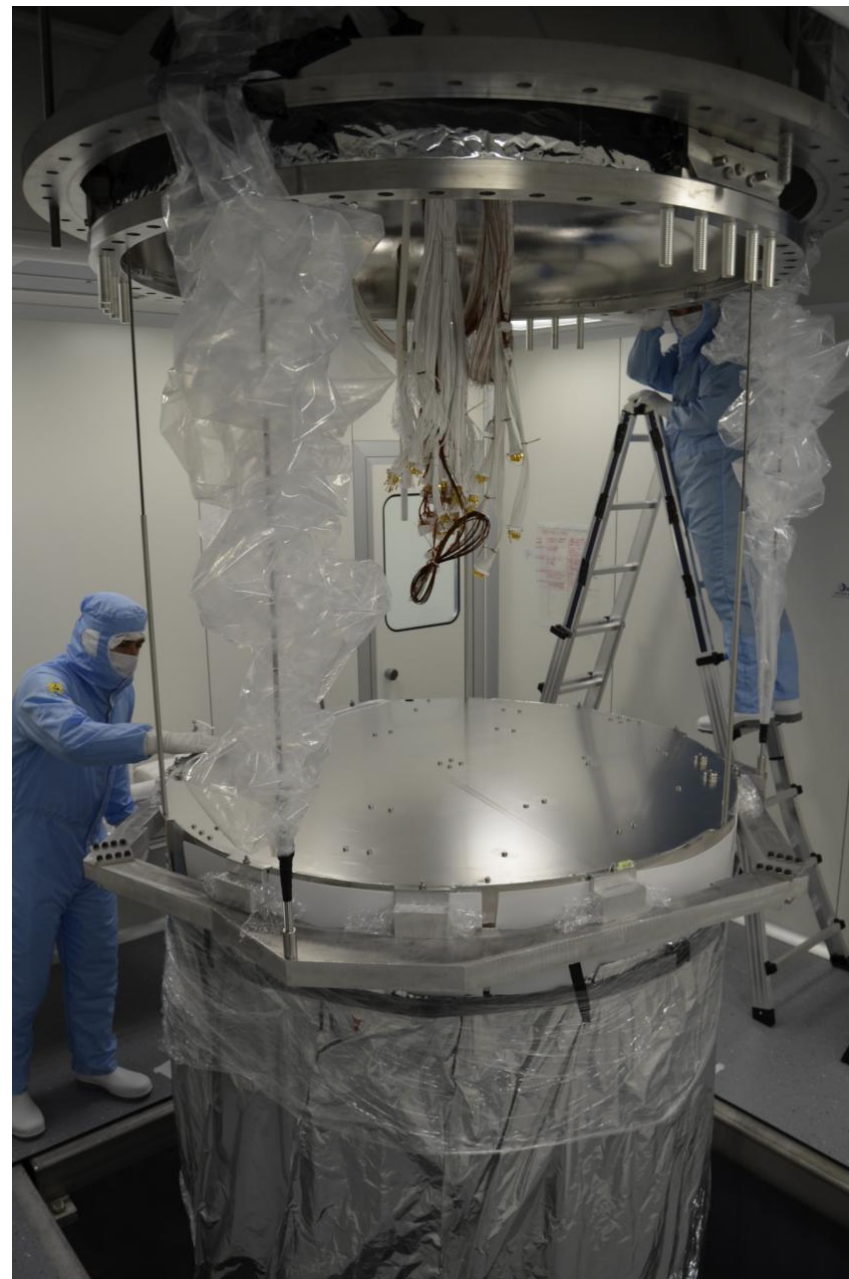
The assembly of the TPC was carried out at LNGS from February 24th to March 5th, during 10 intense days.

- PTFE support structure with 48 panels which define the inner region of the detector.
- 71 field shaping rings and 64 copper rings, connected using two independent resistor chains, for electric field uniformity.
- 10 (400-2400) nm transmitting silica fibers for the light calibration system.
- Two screening electrodes, cathode, gate and anode.



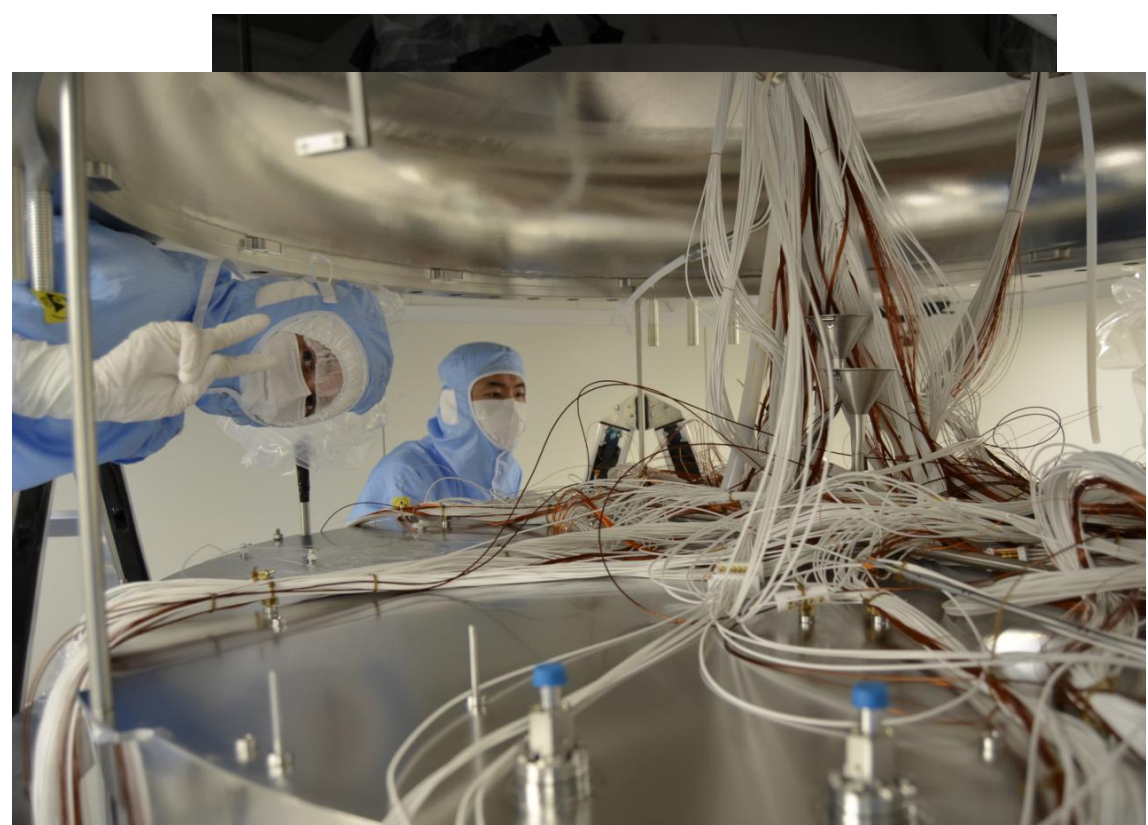
TPC installation underground

- HV and signal cables were tested with a multimeter between the two ends of the cryogenic pipes.
- TPC was brought into the water tank and lifted, into the cleanroom and close to the top of the cryostat to allow cables and fibers connections, as well as other components (e.g. electrodes and level meters).
- TPC was lifted and hanged below the dome. PTFE panels were placed all around the bottom part of the shaping rings as further protection.
- Inner cryostat lifted and tide to the top flange. Later also the outer cryostat has been closed.



TPC installation underground

- HV and signal cables were tested with a multimeter between the two ends of the cryogenic pipes.
- TPC was brought into the water tank and lifted, into the cleanroom and close to the top of the cryostat to allow cables and fibers connections, as well as other components (e.g. electrodes and level meters).
- TPC was lifted and hanged below the dome. PTFE panels were placed all around the bottom part of the shaping rings as further protection.
- Inner cryostat lifted and tide to the top flange. Later also the outer cryostat has been closed.



TPC installation underground

- HV and signal cables were tested with a multimeter between the two ends of the cryogenic pipes.
- TPC was brought into the water tank and lifted, into the cleanroom and close to the top of the cryostat to allow cables and fibers connections, as well as other components (e.g. electrodes and level meters).
- TPC was lifted and hanged below the dome. PTFE panels were placed all around the bottom part of the shaping rings as further protection.
- Inner cryostat lifted and tide to the top flange. Later also the outer cryostat has been closed.



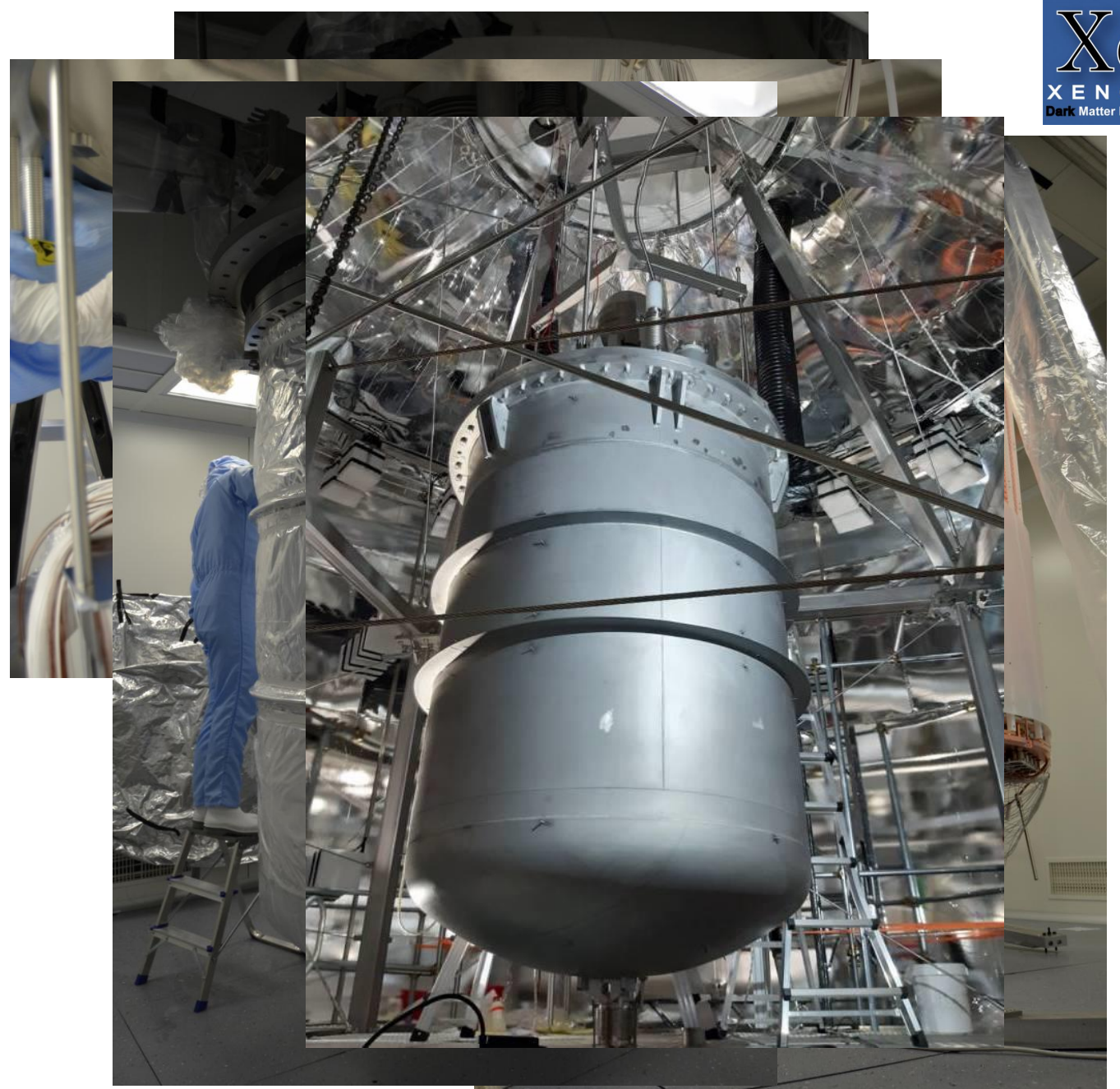
TPC installation underground

- HV and signal cables were tested with a multimeter between the two ends of the cryogenic pipes.
- TPC was brought into the water tank and lifted, into the cleanroom and close to the top of the cryostat to allow cables and fibers connections, as well as other components (e.g. electrodes and level meters).
- TPC was lifted and hanged below the dome. PTFE panels were placed all around the bottom part of the shaping rings as further protection.
- Inner cryostat lifted and tide to the top flange. Later also the outer cryostat has been closed.



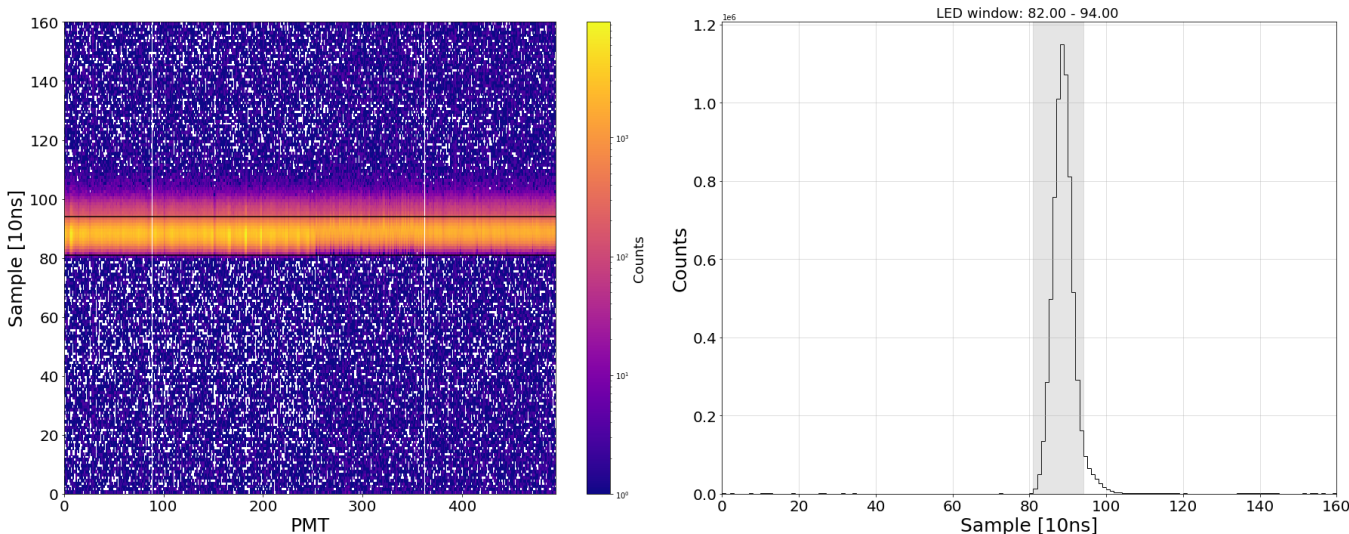
TPC installation underground

- HV and signal cables were tested with a multimeter between the two ends of the cryogenic pipes.
- TPC was brought into the water tank and lifted, into the cleanroom and close to the top of the cryostat to allow cables and fibers connections, as well as other components (e.g. electrodes and level meters).
- TPC was lifted and hanged below the dome. PTFE panels were placed all around the bottom part of the shaping rings as further protection.
- Inner cryostat lifted and tide to the top flange. Later also the outer cryostat has been closed.



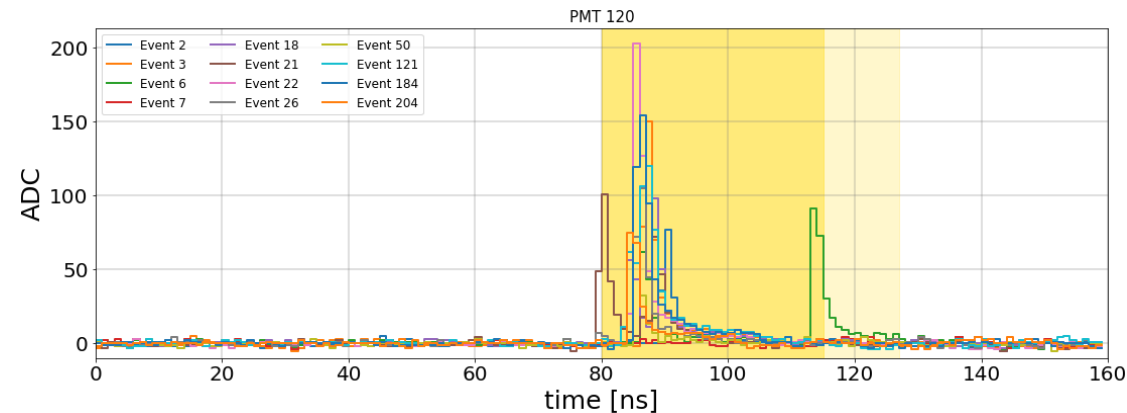
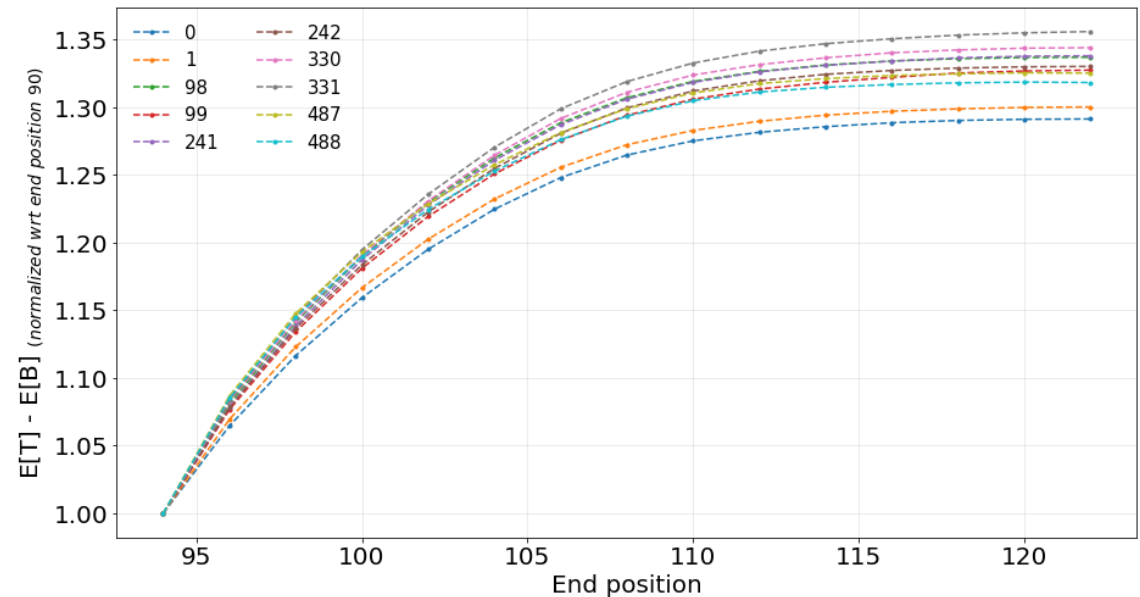
Light calibration system

- Light calibration system for weekly PMT calibration.
- Berkeley Nucleonics Corporation model 505-4c pulse generator to send synchronized pulses to the LEDs.
- The pulse generator, as well as the data acquisition, are externally triggered: $f = 2.4 \text{ kHz}$, $t_{\text{acquisition}} = 1,6 \mu\text{s}$.



Time delay between DAQ trigger and pulse generator trigger has been chosen $8.9 \mu\text{s}$ in order to make the LED signal occurring around the 80th sample.

Processing of raw waveform to compute the area and the amplitude spectrum in given window: optimized to have a 'stable' signal.



Raw waveforms from PMT 120. Integration window in yellow.

Model independent approach for gain calculation

(arXiv:1602.03150v2)

The model independent method estimates the SPE mean statistically without making any assumptions about the underlying shape of the SPE spectrum, but only using the features of signal (T) and noise (B) spectrum.

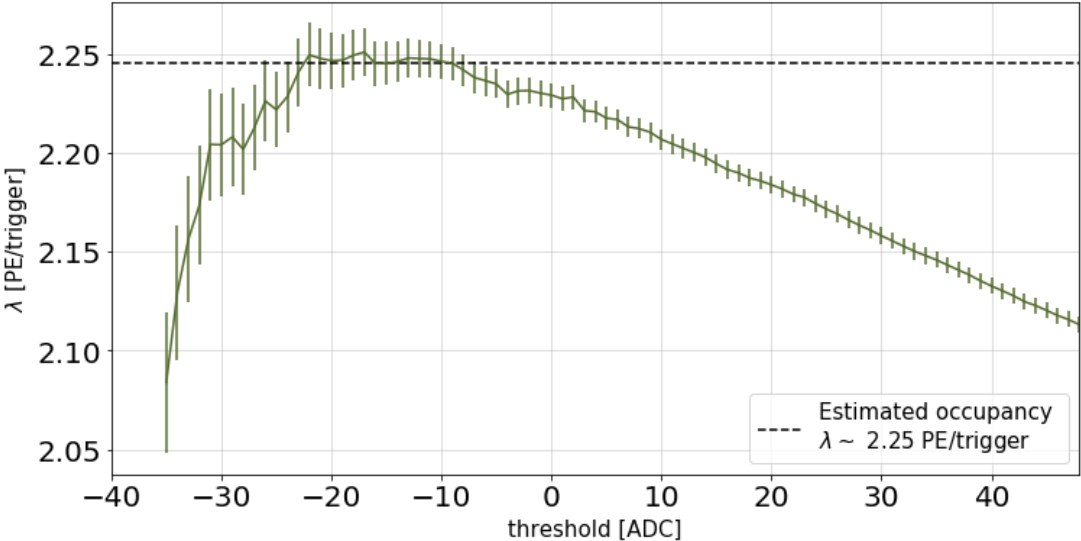
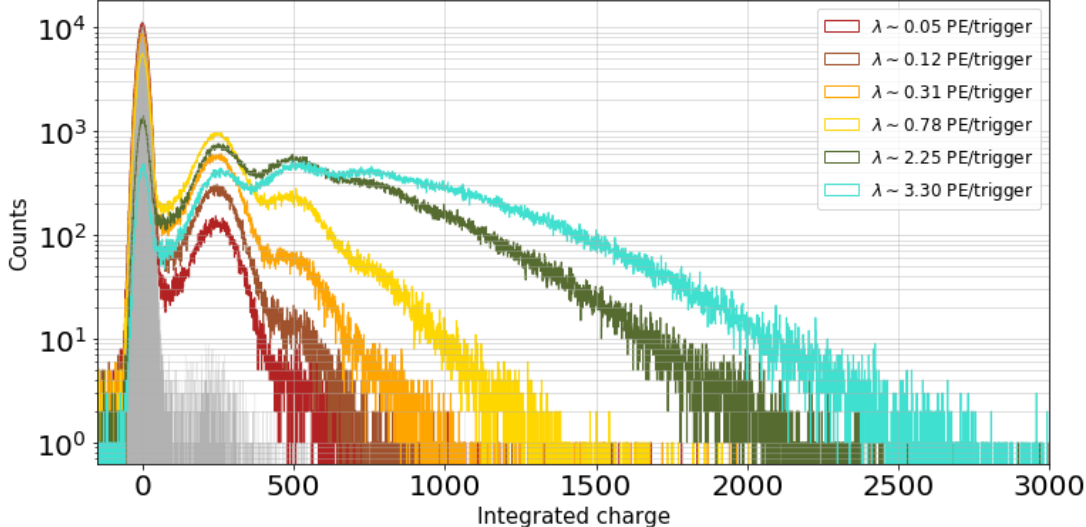
$$E[\varphi] = \frac{E[T] - E[B]}{\lambda} ; \quad V[\varphi] = \frac{V[T] - V[B]}{\lambda} - E[\varphi]^2$$

The only parameter that is not straightforward to estimate is the mean number of laser-induced photoelectrons produced in each trigger λ :

$$L(p) = \frac{\lambda^p e^{-\lambda}}{p!} \longrightarrow \lambda = -\ln(L(0)) = -\ln\left(\frac{N_0}{N}\right) \longleftarrow \frac{N_0}{N} = \frac{A_T}{A_B}$$

The occupancy λ is directly related to the probability of producing zero laser-induced photoelectrons.

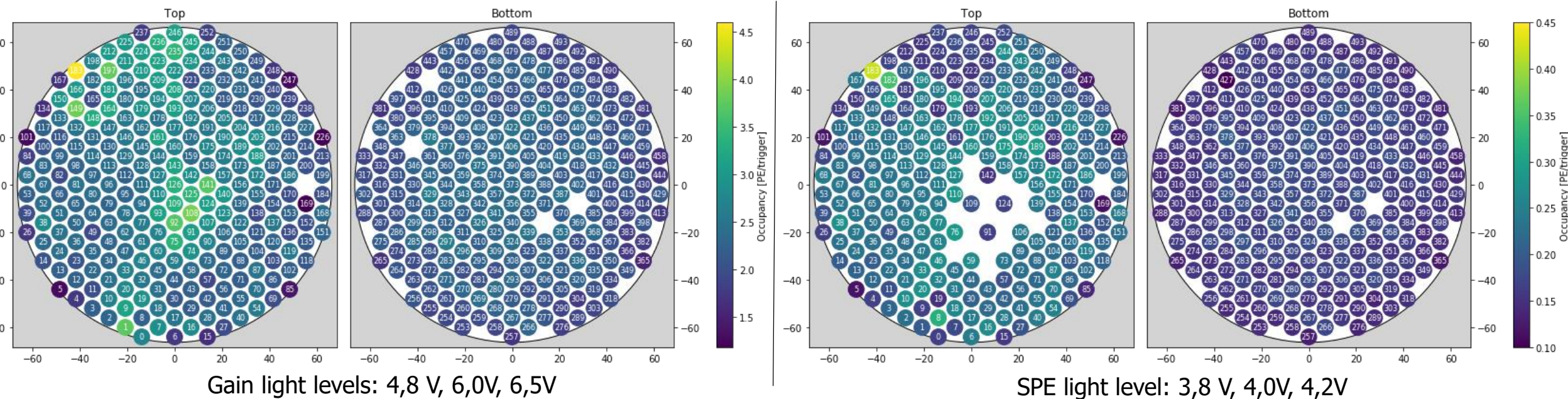
Comparing the number of events in low-charge region of the laser and blank spectrum we estimate the number of zero-pe triggers.



Light levels determination

The gain is estimated through the model independent approach with the average photoelectron per trigger (λ) around ~ 2 PE/trigger, to minimize the systematic uncertainty. The SPE acceptance is defined from the SPE spectrum which needs, in order to minimize the contribution of $PE > 1$, λ less than 0,5 PE/trigger.

LED voltage scan to find the right light settings for gain and SPE acceptance analysis.



High Voltage scan

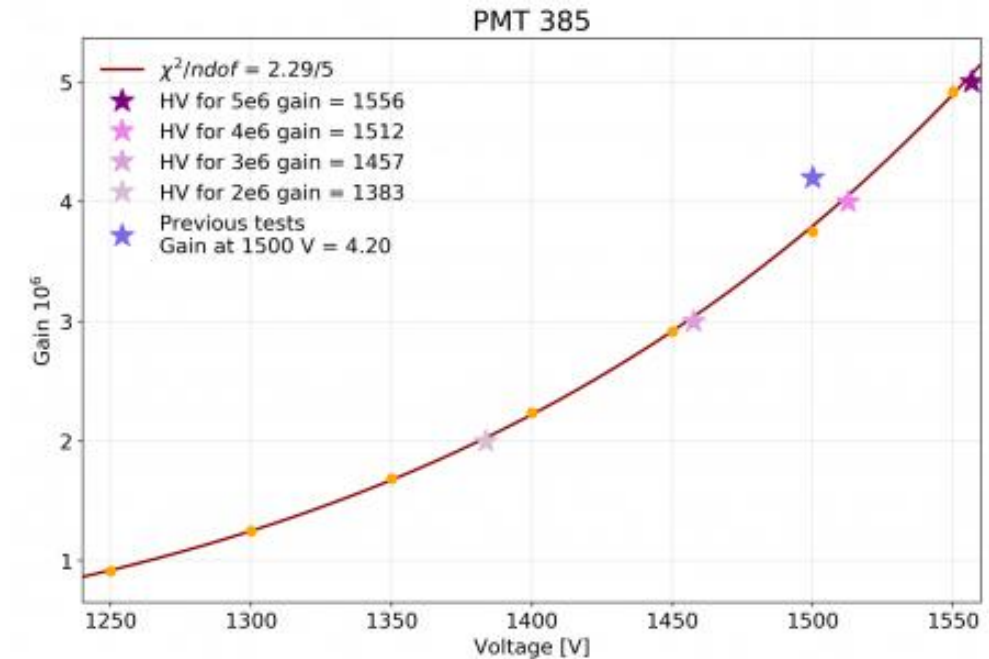
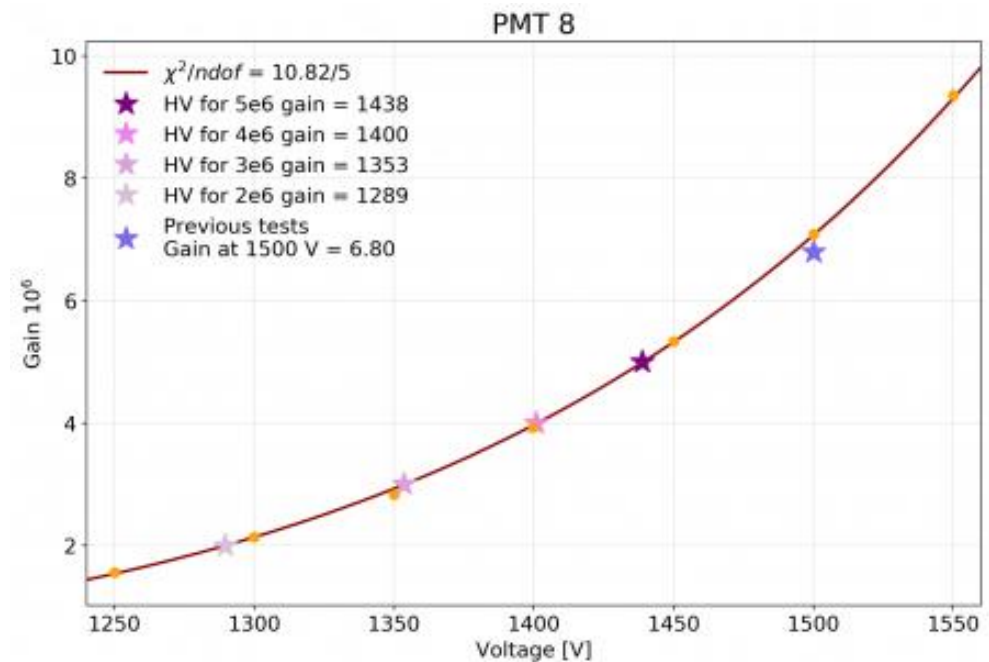
The PMT gain (G) depends on the power supplied (V) to the PMT:

$$G(V) = A \times V^{nk},$$

n is the number of dynodes (n=12) and A, k are parameters typical of every PMTs.

To characterize this function for each PMTs, 7 HV steps of 50 V were used from 1250 V to 1550 V.

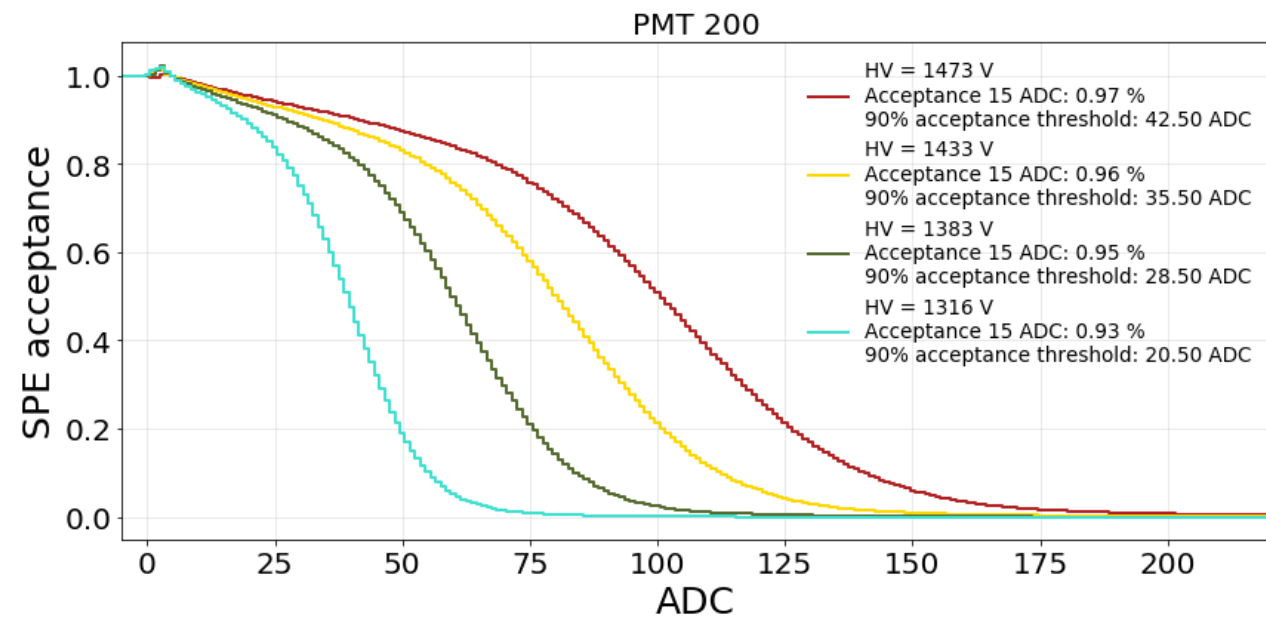
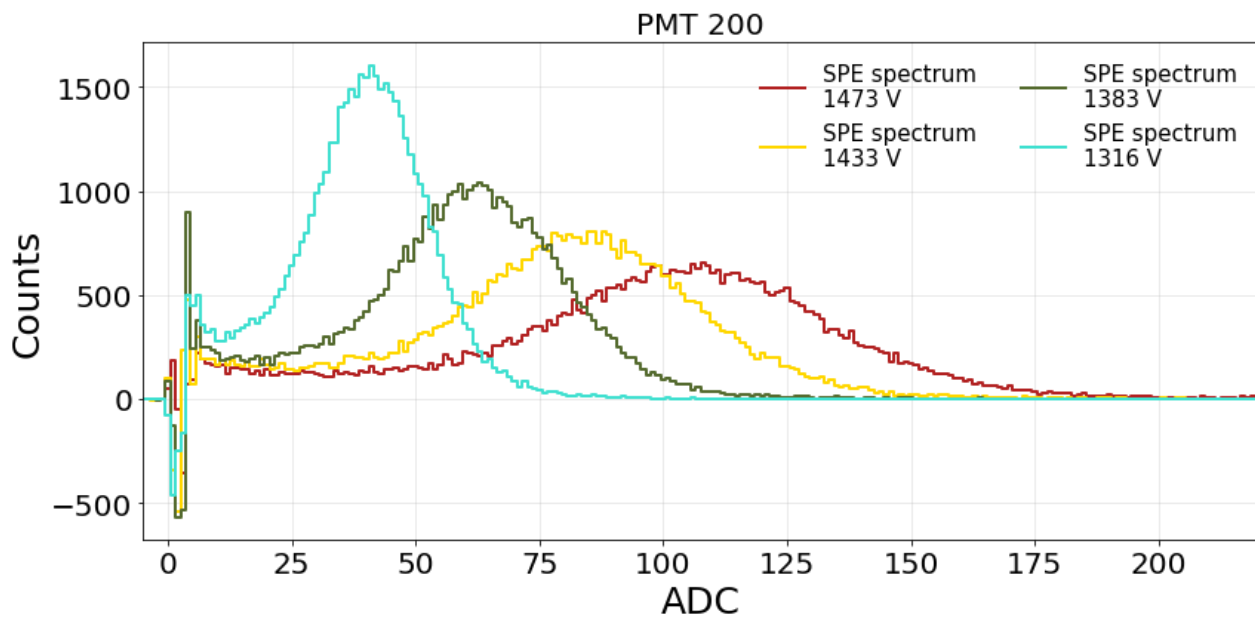
For every PMTs, k and A have been extrapolated from the fit. With this information we can set the HV knowing a priori the gain.



SPE acceptance

In order to increase the discovery power at very low energy it is mandatory to decrease as much as it is possible the energy threshold to include the majority of single photoelectron events (SPE). Then, close to the threshold it is necessary to quantify the SPE acceptance.

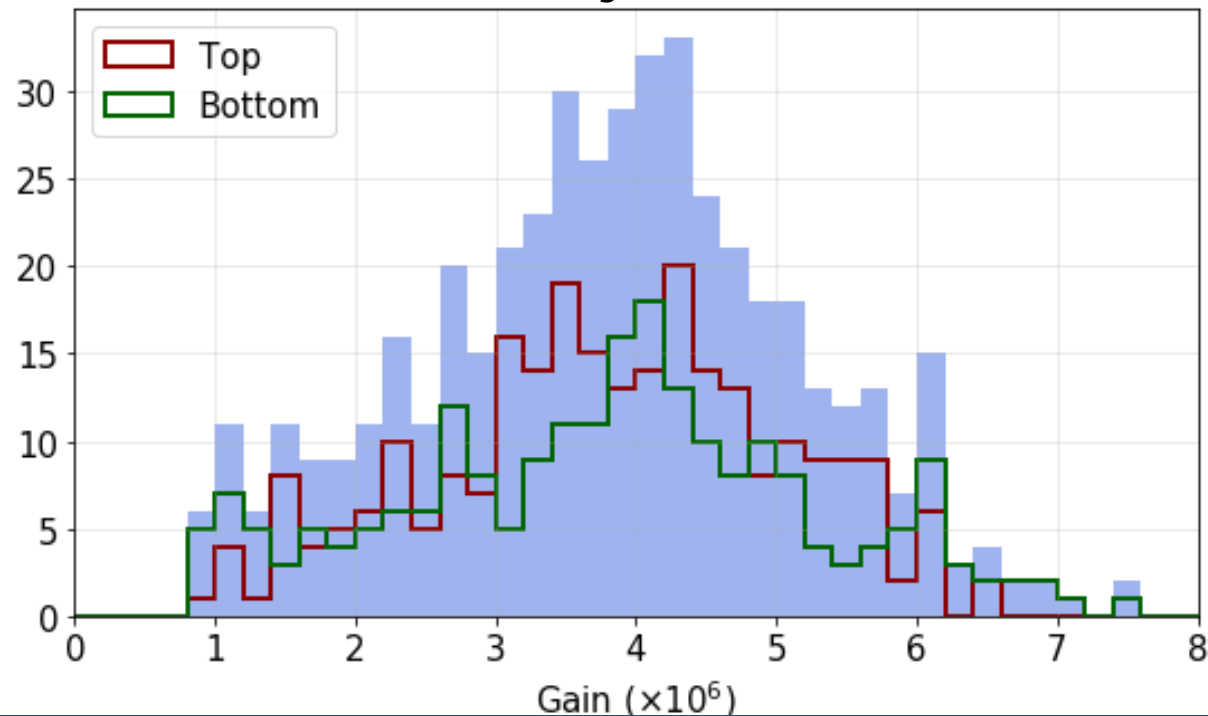
Using the information from the HV scan, the high voltage for equalizing the gain at 2×10^6 , 3×10^6 , 4×10^6 , 5×10^6 has been determined. Using these 4 configurations the SPE acceptance has been studied.



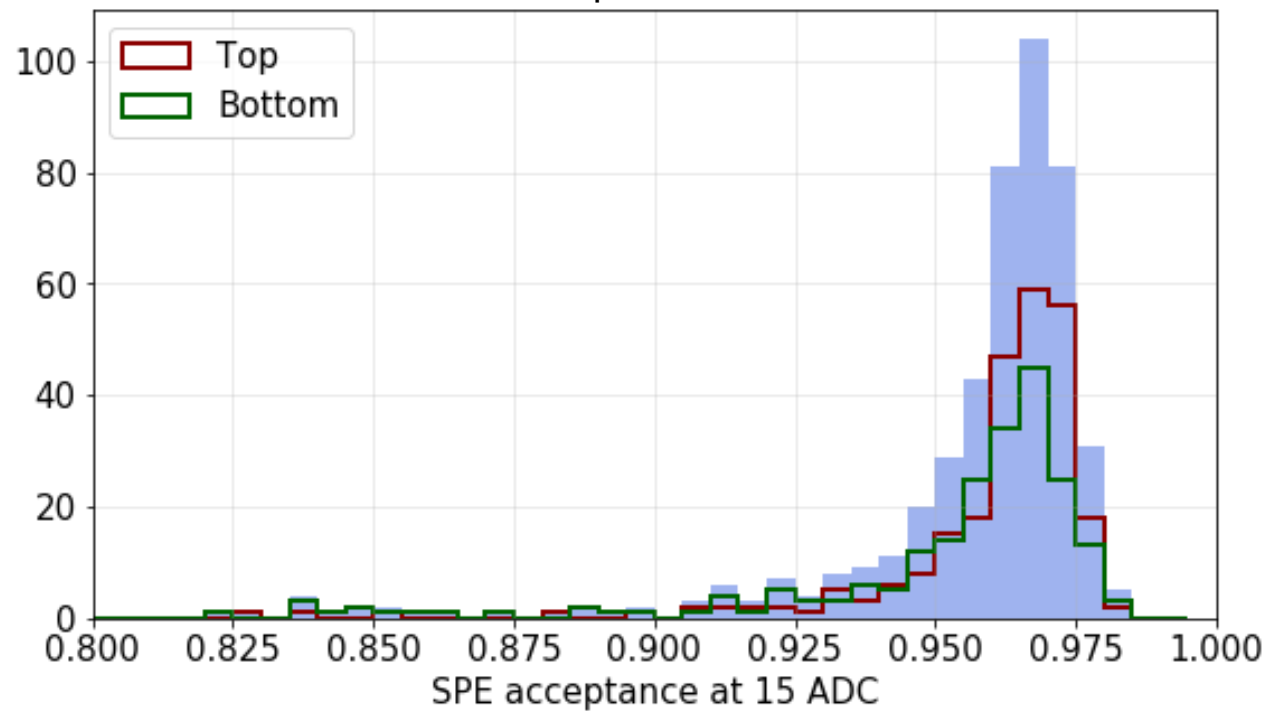
PMT settings for science run

- Equalization of the gain at few million (e.g. $G \approx 4 \times 10^6$) in order to have a uniform detector response.
- Adjustment of the high voltage in order to optimize the SPE acceptance.
- Lowering as much as possible the operational voltage in order to minimize deterioration of performances with time.

XENONnT PMT gain distribution



XENONnT PMT SPE acceptance at 15 ADC distribution



Milestones achieved

- One year and half efforts have been rewarded by completing the TPC assembly.
 - The PMT performances have been deeply studied and their behavior is well understood.
 - We are currently filling the TPC with liquid xenon, while the assembly of the other infrastructures (e.g. neutron veto) are on-going.
-

Outlook

- Characterize the PMTs at the working voltage point in liquid xenon environment.
- Monitoring PMT performances (e.g. gain, AP) with respect the time.
- Parallel PMT related analysis ongoing, e.g. double photoelectron Dark Count characterization.



Thank you for the attention!

XENONnT background

- Radioactive isotopes dissolved in the xenon itself, such as ^{222}Rn and ^{85}Kr , are sources of intrinsic ER background uniformly distributed in the active volume and thus unmitigated by the LXe self-shielding power.
- Irreducible backgrounds arise from interactions induced by neutrinos of solar, atmospheric, or supernova origin. These are spatially uniform due to the small cross-sections involved. Elastic scattering off xenon electrons contributes to the ER background, while coherent elastic neutrino-nucleus scattering (CEvNS) is responsible for an NR background.
- Traces of radioactive isotopes in the detector components close to the active LXe volume can lead to both ER and NR backgrounds

In the energy ROI, the expected ER differential background rate is $13.1 \pm 0.6 \text{ (keV} \times \text{t} \times \text{y)}^{-1}$, a factor 6 lower than the $76 \pm 2 \text{ (keV} \times \text{t} \times \text{y)}^{-1}$ measured in XENON1T. The NR differential background rate amounts to $(2.2 \pm 0.5) \times 10^{-3} \text{ (keV} \times \text{t} \times \text{y)}^{-1}$.

XENON1T results (arXiv:1805.12562v2)

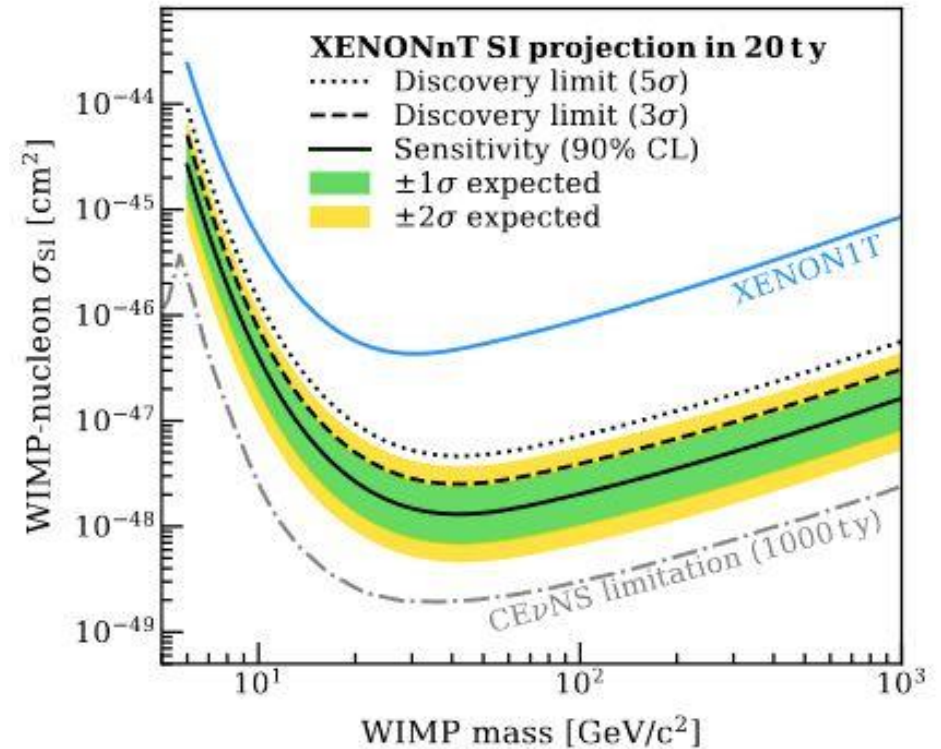
Mass (cS1, cS2 _b)	1.3 t Full	1.3 t Reference	0.9 t Reference	0.65 t Reference
ER	627±18	1.62±0.30	1.12±0.21	0.60±0.13
neutron	1.43±0.66	0.77±0.35	0.41±0.19	0.14±0.07
CEνNS	0.05±0.01	0.03±0.01	0.02	0.01
AC	0.47 ^{+0.27} _{-0.00}	0.10 ^{+0.06} _{-0.00}	0.06 ^{+0.03} _{-0.00}	0.04 ^{+0.02} _{-0.00}
Surface	106±8	4.84±0.40	0.02	0.01
Total BG	735±20	7.36±0.61	1.62±0.28	0.80±0.14
WIMP _{best-fit}	3.56	1.70	1.16	0.83
Data	739	14	2	2

Model component	Expectation value (μ) in 20 ty		Rate uncertainty (ξ)
	Observable ROI	Reference signal region	
Background			
ER	2610	1.69	
Neutrons	0.29	0.15	50%
CEνNS (Solar ν)	7.61	5.41	4%
CEνNS (Atm+DSN)	0.82	0.36	20%
WIMP signal			
6 GeV/c ² ($\sigma_{\text{DM}} = 3 \times 10^{-44} \text{ cm}^2$)	25	19	
50 GeV/c ² ($\sigma_{\text{DM}} = 5 \times 10^{-47} \text{ cm}^2$)	186	88	
1 TeV/c ² ($\sigma_{\text{DM}} = 8 \times 10^{-46} \text{ cm}^2$)	286	118	

Projections of the XENONnT sensitivity and discovery power in the search for spin-independent WIMP-nucleon couplings

XENONnT projected sensitivity

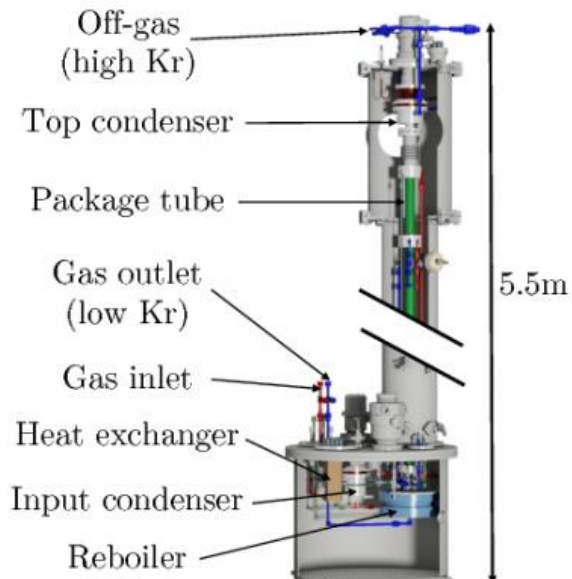
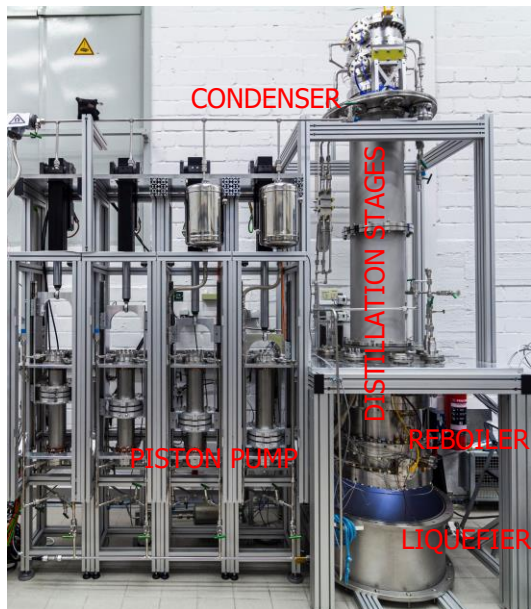
- Energy region of interest: (1, 13) keV and (4, 50) keV for electronic and nuclear recoils.
- Expected average differential background (4 t fiducial mass):
 - $B_{ER} = 13.1 \pm 0.6 \text{ (keV} \times \text{t} \times \text{y)}^{-1}$;
 - $B_{NR} = (2.2 \pm 0.5) \times 10^{-3} \text{ (keV} \times \text{t} \times \text{y)}^{-1}$.
- With the exposure goal of 20 t×y, the expected sensitivity to spin-independent WIMP-nucleon interactions reaches a cross-section of $1.4 \times 10^{-48} \text{ cm}^2$ for a 50 GeV/c² mass WIMP at 90% confidence level.



Source	Rate [(t×y) ⁻¹]	Source	Rate [(t×y) ⁻¹]	Source	Rate [(t×y) ⁻¹]
Detector radioactivity	25 ± 3	¹³⁶ Xe	16 ± 2	Neutrons	(4.1 ± 2.1) × 10 ⁻²
²²² Rn	66 ± 7	¹²⁴ Xe	4 ± 1	CEvNS (solar ν)	(6.3 ± 0.3) × 10 ⁻³
⁸⁵ Kr	13 ± 1	Solar ν	34 ± 1	CEvNs (Atm + DNS)	(5.4 ± 1.1) × 10 ⁻²

Estimated background event rates in the 4 t fiducial volume of XENONnT, based on the energy of the recoil even (arXiv:2007.08796v1).

XENONnT purification system



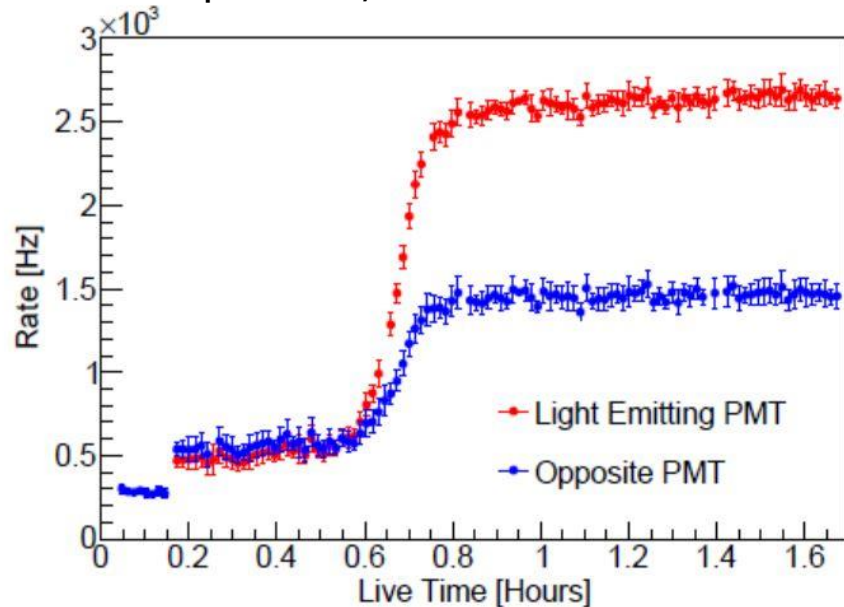
Radon and Krypton distillation columns.

- The system demonstrated a krypton reduction factor of 6.4×10^5 with thermodynamic stability at process speeds above 3 kg/h. The resulting concentration achieved in XENON1T ($^{\text{nat}}\text{Kr}/\text{Xe} < 26$ ppq) is the lowest ever achieved (Eur. Phys. J. C (2017) 77:275).
- Aim for the reduction by a factor of 10 w.r.t. XENON1T down to $1 \mu\text{Bq} / \text{kg}$ by: screening and avoiding radon, meticulous cleaning campaigns, better surface-to-volume ratio, high-flux radon distillation column

Electronegative impurity removed in the purification line to increase the amount of free charges detected.
 New liquid purification line together with the existing gas purification line.

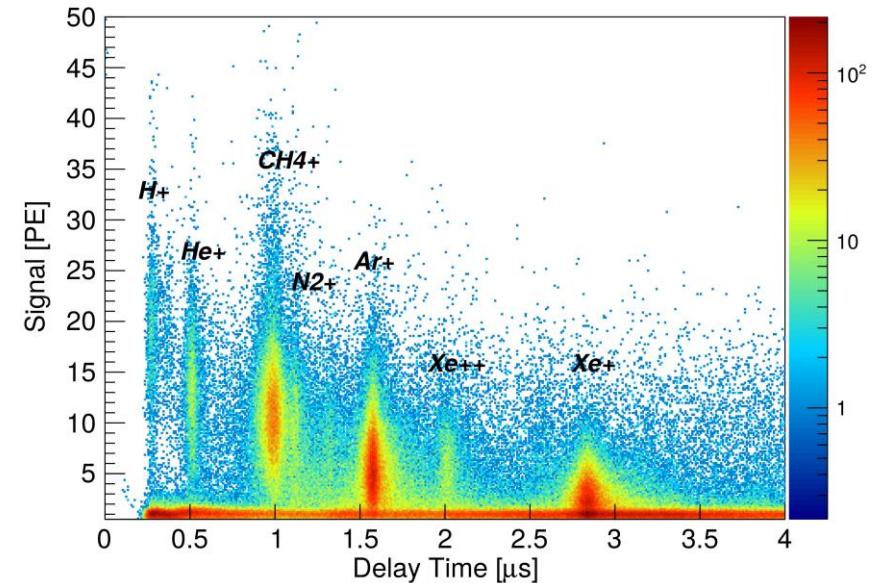
PMT test: after-pulses and light emission

- Two arrays facing each other allows us to investigate the possible light emission: high local electric fields inside the PMT can produce small discharges.
- This effect is strongly voltage dependent and can be measured at liquid xenon temperature, due to the absence of the thermionic emission



The dark count rate of two facing PMTs over time. The light emitting PMT (red points) emits light as soon it is turned on, and the no-light emitting PMT (blue points) receives the light.

Delay time spectrum of a R11410-21 PMT at a bias voltage of -1500 V.



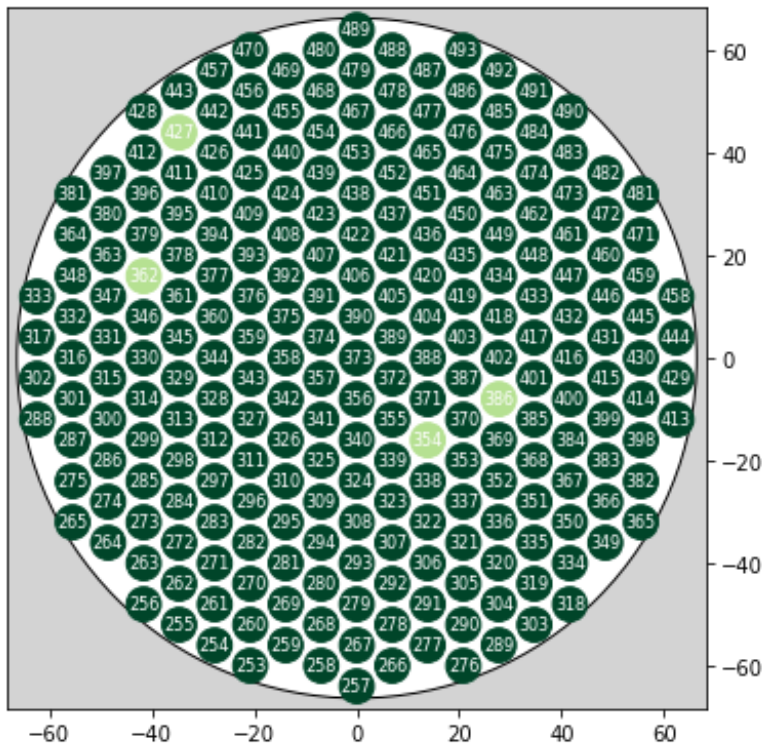
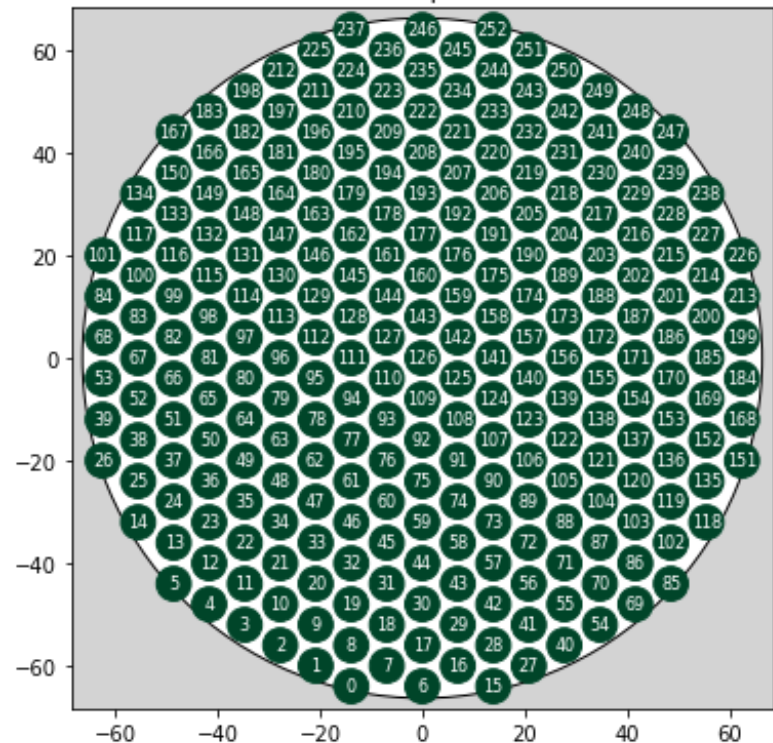
- PMTs are evacuated, in order to increase the free mean path of the electrons, and thus to limit the interactions of the electrons with the residual gas.
- Photoelectrons and secondary electrons produced by an incident photon can hit a single gas molecule along their trajectory and ionise it. Due to its positive charge, the produced ion travels back to the photocathode and with its kinetic energy releases free electrons into the vacuum.

$$t_{Delay} = C(V) \sqrt{\frac{M}{Q}} [\mu s]$$

XENONnT PMT: current status

Top

Bottom



All PMTs are working besides PMT numbers 354, 362, 386, and 427.

